International Journal of Engineering and Technology Innovation, vol. 14, no. 4, 2024, pp. 355-377

Optimizing Seismic Design of Multi-Tower Buildings Using Sky Bridge Isolation and BIM: A Case Study

Michael Loreantz Steven Tambunan[1], Jessica Sjah[1,*], Ayomi Dita Rarasati[1], Ryan Sulistian[1], Bambang Trigunarsyah[2]

[1]Department of Civil Engineering, Faculty of Engineering, Universitas Indonesia, Depok, Indonesia

[2]School of Property, Construction and Project Management, RMIT University, Melbourne, Australia

Received 25 February 2024; received in revised form 05 May 2024; accepted 06 May 2024

DOI: https://doi.org/10.46604/ijeti.2024.13409

Abstract

This research aims to extend prior knowledge of sky bridge isolations in a design case study that complies with building codes, focusing on the design of a multi-tower building linked with a sky bridge and its isolation system. Building Information Modeling (BIM) is used during the design process. Linear time history analysis is performed to capture seismic responses without statistical distortion of response combinations. Link elements are used to simulate the isolations, and the ground motions are excited in bidirectional directions. The experimental results demonstrate that using an isolation system at the sky bridge connection improves torsional behavior, as evidenced by a 12% reduction in torsional mass contribution in the fundamental mode shape of the buildings. Other notable improvements include better lateral force distributions and optimization of reinforcement volume by 36.91% at maximum. Additionally, convenient post-design procedures, such as automated design visualizations and quantity surveys of reinforcements are reported through using BIM.

Keywords: Building Information Modeling (BIM), multi-tower, seismic design, seismic isolation, sky bridge

1. Introduction

Multi-tower building structures are often characterized by two separate buildings linked by a connecting element, such as a podium structure at lower elevations [1]. Li et al. [2] mentioned that these multi-tower structures respond to the demand of urban development for multifunctional high-rise buildings. Opposed to podium structures, sky bridges may be utilized to connect multi-tower building structures at higher elevations [3]. The utilization of sky bridges itself offers notable benefits, including enhanced mobility for building users and facilitating efficient movement throughout the building [4]. Statistical evidence also suggests that sky bridges can improve evacuation efficiency during emergency scenarios by up to 30% [5]. However, significant changes are noted in the seismic responses of two building structures connected with a sky bridge, particularly in terms of base shear response and structural drifts [6].

In practical applications, an isolation system can enhance a structure's performance under seismic loads by modifying its inertial response and improving energy dissipation properties. Chen and Xiong [7] showed that using an isolation system at the base level of a building may reduce its acceleration demands. Jara et al. [8] further showed not only acceleration demands but also drift demands may be improved through the use of isolation. Zhang and Ali [9] mentioned that energy dissipation may be improved through slight movements offered by isolations. This endeavor to dissipate energy is particularly beneficial in seismic-prone areas, where building collapses during earthquake events often result in casualties [10].

* Corresponding author. E-mail address: jessicasjah@ui.ac.id

English language proofreader: Yen-Chun Hsieh

Several forms of seismic isolation systems have been researched previously for different usages and effectiveness in achieving previously mentioned benefits. Numayr et al. [11] performed a comparison study of lead rubber bearings, high-damping rubber bearings, and coil springs as a base isolator for an asymmetric building foundation. It is reported that the high-damping rubber bearing alternative performed the best in reducing inter-story displacements due to a certain ground motion. Hosseini and Soroor [12] noted the high economic cost of rubber bearing. The research presented a roller isolator with the capability of releasing bi-directional horizontal movement only as seen in Fig. 1, making it feasible in seismic usage with unpredictable direction of excitation.

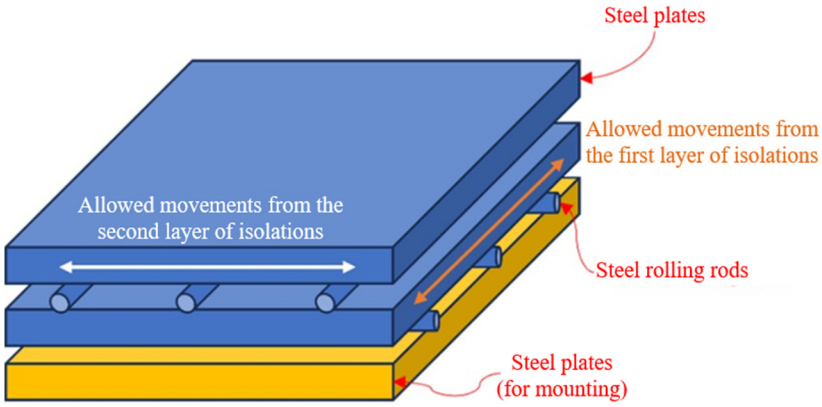

Fig. 1 Bidirectional isolation system (Adopted from [12])

It is noted that isolation systems are not the only feasible way to improve the seismic resistance of a structure. For instance, recent studies have been made in multi-layer periodic unit cells to obtain the benefits of using isolation systems [13]. This concept of unit cells may be applied to multi-tower structures as it is composed of structural elements resembling the unit cells. When designed properly, the concept may hypothetically introduce the benefits of isolation systems without explicit use of isolations.

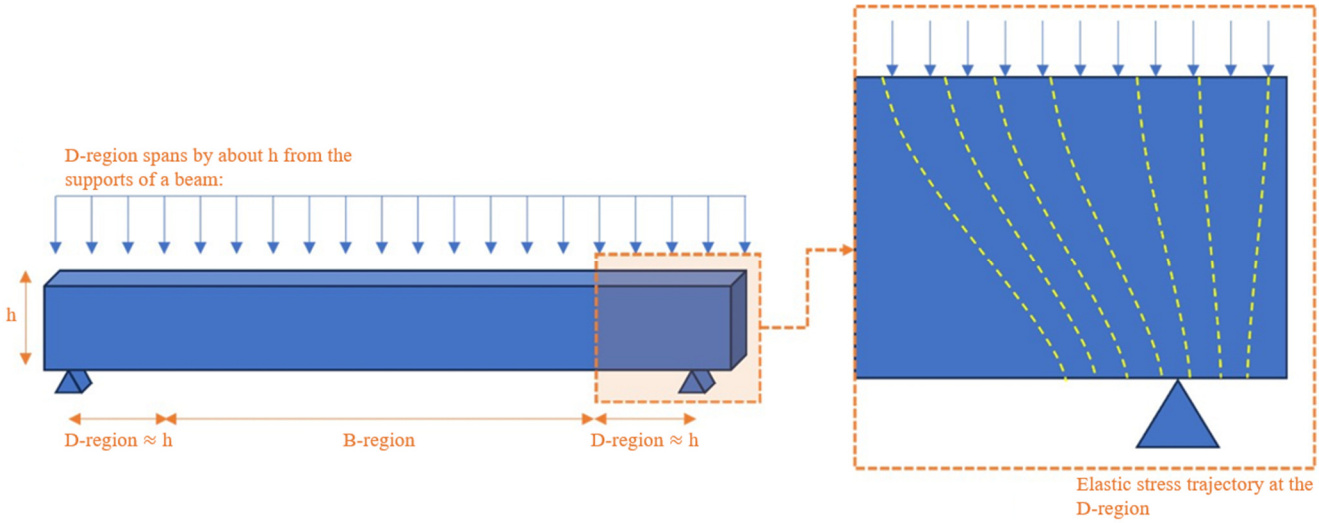

Fig. 2 Visualization of B-region and D-region

The topic of B-region and D-region is an important starting point for discussing local responses of sky bridge. The terms B-regions and D-regions are mainly used in concrete design to assess the local behaviors of an element based on the occurrence of stress concentrations [14]. B-region stands for Beam or Bernoulli region, a region where elastic stress trajectory varies linearly. D-region on the other hand stands for Disturbed or Discontinued region, a region where elastic stress trajectory varies non-linearly due to the significant stress concentrations following Saint-Venant's principles. In a beam system, the D-region spans by about the beam depth from the support of the beams [15]. A visual representation of the positions of B-region and D-region positions in a beam system may be seen in Fig. 2. Considering a sky bridge system highly resembles the system in the

figure, it is concluded that the ends of the sky bridge may be classified as D-region. The usage of isolation may not only benefit the global response in designing the whole structure but may also benefit the sky bridge design locally through the reduction of stress concentrations.

Several studies in seismic isolations for connecting structures in adjacent buildings are noted to have been conducted previously. Wu et al. [16] proposed optimum analytical formulas for viscoelastic dampers and viscous fluid dampers for sky bridges. In obtaining the formulas, numerical simulations using 2-bay linear-elastic frames were conducted to obtain optimum inter-story displacements. Lee et al. [17] implemented variations of isolation systems in 42-stories and 49-stories buildings in Seoul, South Korea. It was found from the research that bearing-type isolation systems could significantly improve the damping properties of linked buildings. The interest of the research however was limited to analyzing the improvements in seismic behaviors of the two buildings. Effects of isolations in sky bridge systems on the whole structural design such as reinforcement efficiency in multi-tower buildings are yet to be done.

Guo et al. [18] further assessed the benefits of a novel isolation system, namely negative stiffness dampers, in the nonlinear performance of multi-tower buildings. The research reported improvement in structural damage is seen by the usage of isolation. The findings, however, were obtained in steel structures only and not calibrated with building design codes. The most recent study in the field of isolated sky bridges is noted to be conducted by Zhang et al. [19]. The research proposed a novel numerical model of a tuned inerter damper connecting two separate structures. The research unfortunately was limited to numerical analysis in 2-dimensional sway frames with no applied studies in structural design.

For discussions in building design and construction, the design stage is widely recognized as a time-consuming process due to the necessity of integrating various disciplines [20]. Gartoumi et al. [21] noted that the inefficiencies emerge due to the traditional construction practices that mostly rely on two-dimensional information modeling. In the context of the design process of buildings, such forms of inefficiencies may include design errors, inability to detect engineering faults, and difficulty in deciding design options. Building Information Modeling (BIM) on the other hand focuses on three-dimensional information modeling of construction projects, regarded as a remedy for issues inherent in current construction practices [22].

Previously, BIM has been utilized for material quantity calculations using software like Autodesk Revit [23]. BIM continues to evolve now, with applications extending beyond new building designs to encompass structural retrofitting as well [24]. Furthermore, BIM is increasingly employed not only to support construction projects but also to generate system diversifications within facilities [25]. Regarding BIM usage in multi-tower structure design connected with sky bridges, Brooker and Lin [26] mentioned the use of BIM for designing the façade system in DJI Headquarters, China. Veall et al. [27] also published that BIM was used in the structural design of Atlantis The Royal building in Dubai. However, the extent of the BIM usage was not explicitly elaborated in both papers.

The literature reveals that several studies have been conducted in optimizing structural response through the usage of isolations. However, practical application of the knowledge of sky bridge isolations to the extent of structural design complying with design codes has yet to be done. This research aims to extend the previous research through a concise case study of a multi-tower building in a seismic-governed zone. It is also noted that the structural design process may be improved significantly through the current development of BIM. Knowing this, BIM in this research is used for optimizing the process of reinforcement detailing, design visualizations, and reinforcement volume calculations. Comparisons of structural responses and optimizations in reinforcement volumes of beams, columns, and slabs are reported before and after the introduction of the isolation system to the sky bridge connection. Findings in this research are expected to provide practicing engineers in the building design industry with the advantages and potential design drawbacks of employing sky bridge isolation in multi-tower buildings as interconnected structures.

2. Research Methodology

The research started with literature reviews regarding related topics of multi-tower, BIM, and isolation systems. A review of completed architectural data was conducted as a basis of structural design in this research. Sizing of elements and structural framing generation was done in Autodesk Revit followed by structural analysis of the analytical model using ETABS. Isolation constraints were then introduced in ETABS before the analysis and reinforcement design phase. Obtained reinforcements are then transferred as a full BIM model to Autodesk Revit for the quantity surveys and presentation of designs. For clarity, the research flowchart is presented in Fig. 3.

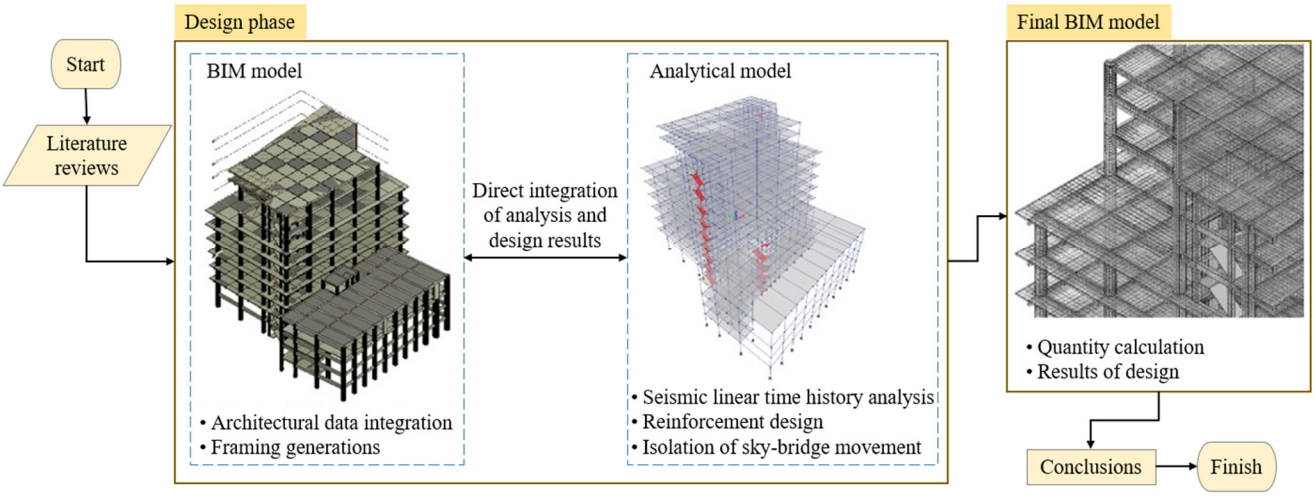

Fig. 3 Research flowchart

The focus of this study is on two laboratory building structures linked by a sky bridge, shown in detail in Fig. 4. The building is designed to be built in Depok, Indonesia. Seismic load mainly governs the lateral design of the buildings due to the high seismic nature of the site location. On the left side of Fig. 4(a) stands Tower Laboratory, a 10-story building with a roof elevation of 39.7 m above ground level. Designed as the primary laboratory facility, Tower Laboratory boasts a floor plan area ranging from 854 m^2 at higher elevations to 1204 m^2 at lower elevations.

On the right side of Fig. 4(a) lies Hangar Laboratory, a 5-story building with a roof elevation of 19.2 m above ground level. This structure serves as a large-scale testing facility, featuring a significant opening that accounts for 64.9% of the total floor plan dimension of 800 m^2. The plan involves connecting both structures via a sky bridge, positioned between the second and third stories of each respective building. Due to differences in structural floor elevations, the sky bridge exhibits a 5° inclination along its longitudinal axes. Moreover, variations in the buildings' orientations result in differing spans along the sky bridge plane, with a maximum span of 6.06 m at one end and a minimum span of 5.38 m on the other ends. Detailed schematics regarding the research object may be evaluated in Fig. 4 below.

The design process is carried out using ASCE 7-16 standards for the loading criteria and ACI 318M-14 for the concrete design procedure. The choices of these standards are due to the current Indonesian building codes that refer directly to American building codes. Linear time history analysis is used in analyzing and designing the structure, with skeletal elements of the structure (beams and columns) modeled as frame elements. Considering the usage purpose of the buildings as a laboratory, a uniform live load of 5 kPa is used with a risk category that falls into the IV category of ASCE 7-16. The decision to classify the structure as Category IV is due to the importance of the structure as a teaching facility. Due to its risk category, the earthquake load demand increases by about 150% as required by the importance factor I_e. Further considering architectural requirements, the structure was designed using only an open-frame structural system. The full seismic loading parameters that were used in designing the structure may be evaluated in the Appendix of Table A1.

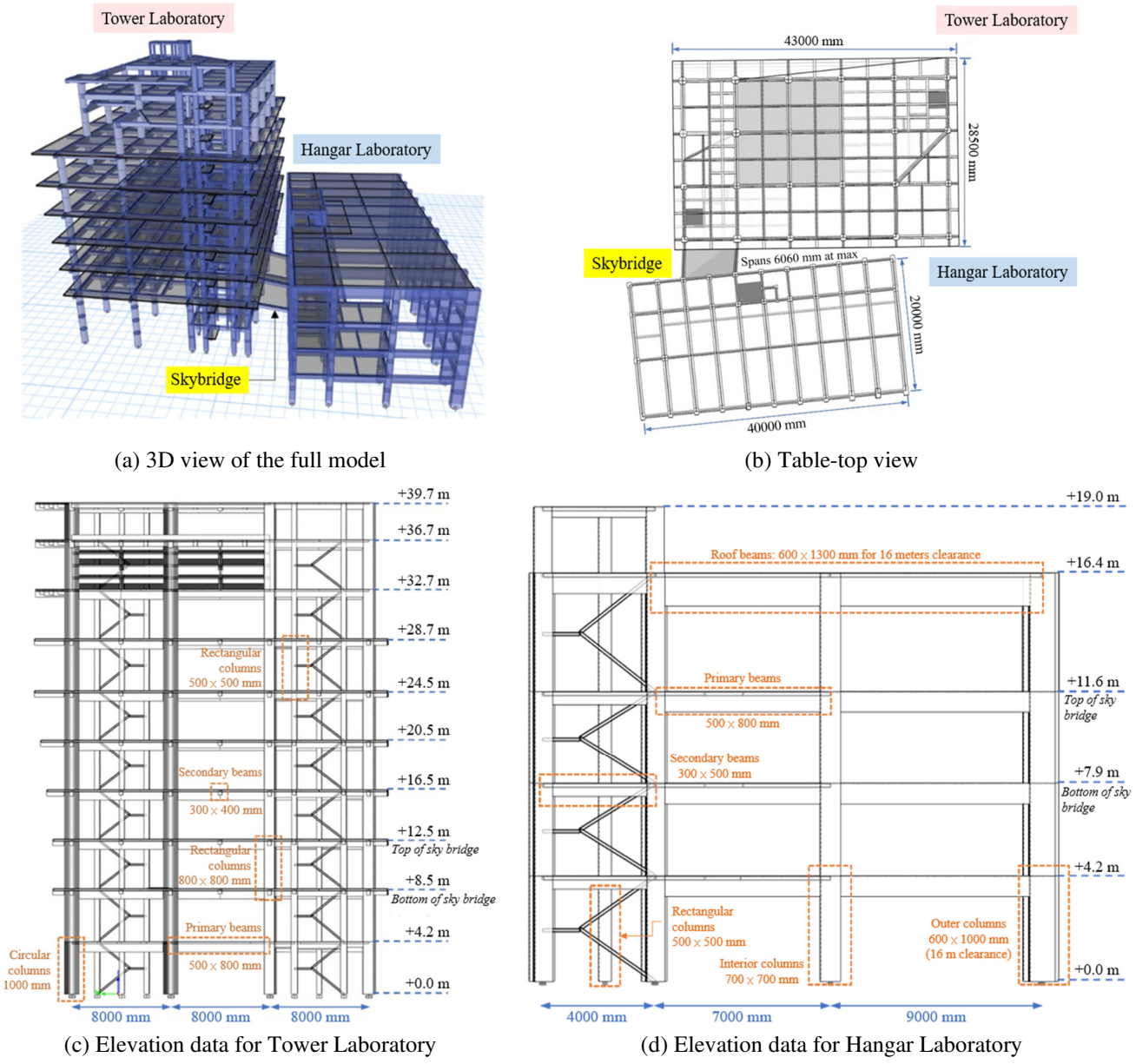

(a) 3D view of the full model

(b) Table-top view

(c) Elevation data for Tower Laboratory

(d) Elevation data for Hangar Laboratory

Fig. 4 Research objects

A circular cross-section of 1000 mm in diameter and a rectangular cross-section of 600 mm × 1000 mm are used for the dimensions of the columns in this study. The dimensions of rectangular beams vary from 300 mm × 400 mm to 600 mm × 1300 mm, corresponding to the required load demands for each beam. Slabs were modeled as a shell-thin element with 130 mm thickness. These element choices have been verified to comply with ACI 318M-14 Standards for a special moment resisting frame system. The sizing of these elements is also chosen to fulfill the required drift limits, constrained by the risk category and structural system mentioned before. A visual representation regarding the element sizing and their respective positions may be evaluated briefly in Fig. 4(c) for the Tower Laboratory, and in Fig. 4(d) for the Hangar Laboratory. All structural elements are designed using concrete as the main material. Concrete material is modeled as an isotropic material and its properties are specified in Table 1.

Table 1 Material properties of concrete

Variables	Values
Compressive strength (f_c')	35 MPa
Weight density	24 kN/m^3
Modulus of elasticity (E)	27806 MPa
Poisson's ratio (v)	0.2
Shear modulus (G)	11913 MPa

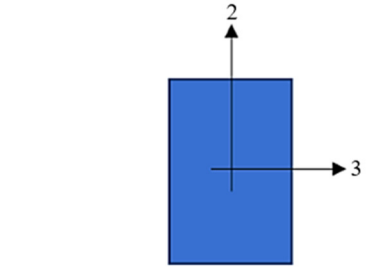

Cracked section stiffness reduction for linear analysis
(Adopted from ACI 318M-14)

Element	Stiffness reduction
Beam	$I_{22} = 0.35\ I_{gross}$; $I_{33} = 0.35\ I_{gross}$; $I_{torsion} = 0.1\ I_{gross}$
Column	$I_{22} = 0.70\ I_{gross}$; $I_{33} = 0.70\ I_{gross}$
Slabs	$I_{in\text{-}plane} = I_{out\text{-}of\text{-}plane} = 0.25\ I_{gross}$

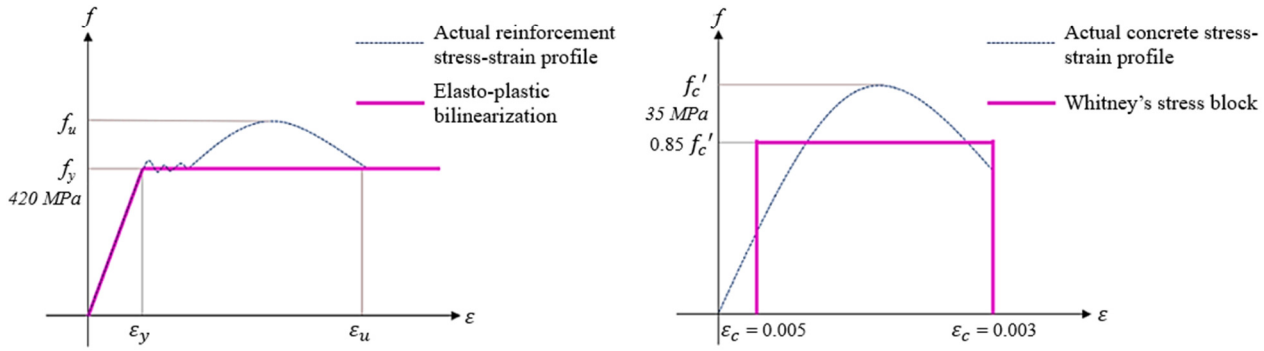

Fig. 5 Parameters for material non-linearities

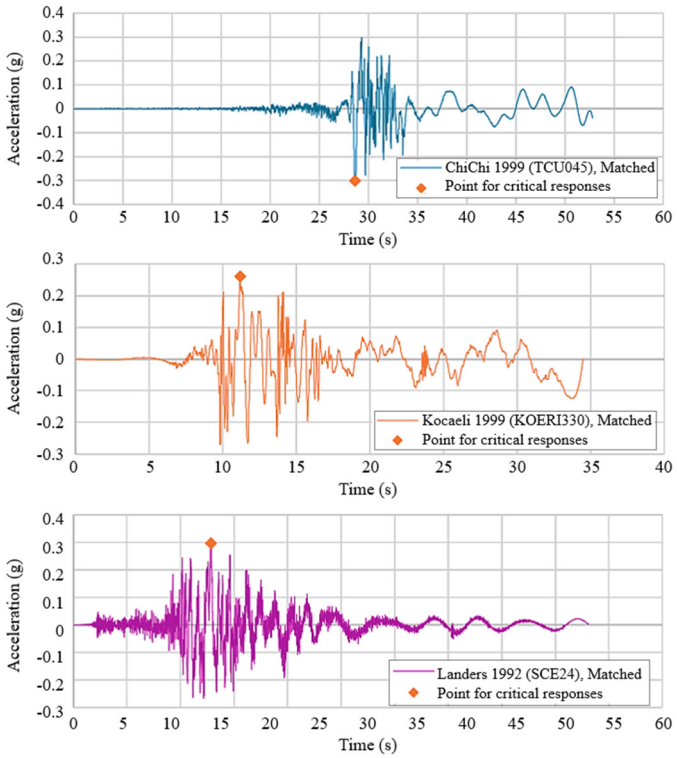

(a) Spectrally matched ground motions

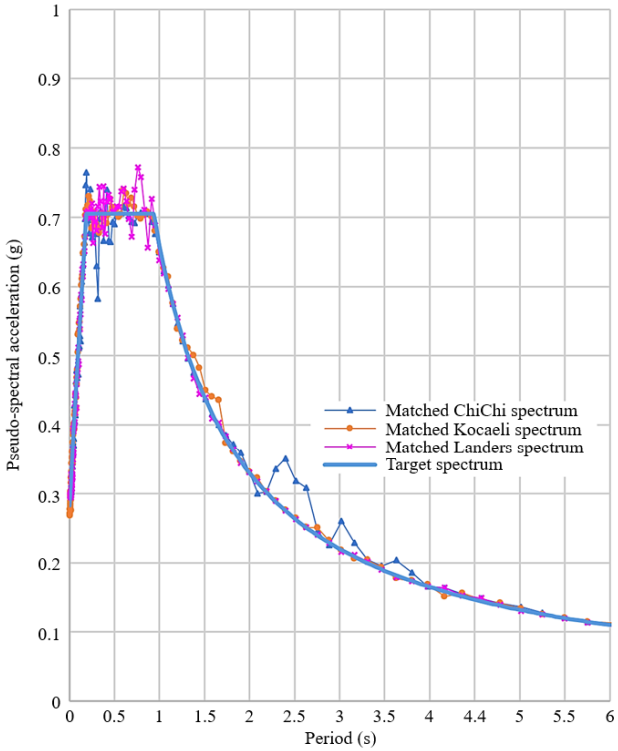

(b) Response spectrum for each matched ground motion

Fig. 6 Ground motion data (initial data adopted from PEER Ground Motion Database)

Material non-linearities during the linear analysis are considered implicitly through stiffness reduction of concrete cracked sections. Further following current practices in building design, expected earthquake load demand is also reduced to take account of the structural ductility through the response modification factor R. Explicit consideration of the material non-linearities are then used during the design procedures of beam, columns, and slabs through idealized stress-strain relationships. A visual representation of the stiffness reduction and material stress-strain relationships may be evaluated in Fig. 5.

For linear time history analysis, seismic risk deaggregation utilizes Indonesia's seismic hazard map, with Depok (Indonesia) selected as the site location of the multi-tower building. The ground motion data was to be selected from the PEER Ground Motion Database. The database itself requires specific site information such as return period, earthquake sources, and

more as specified in the Appendix of Table A2. The return period is taken as 2500 years due to the exceedance period of the MCE_R spectrum is 5% for 500 years. Other information such as earthquake mechanisms and distance of earthquakes are taken statistically from the hazard map specifically to the site location of the building.

As required by ASCE 7-16, a minimum of three ground motions were selected to carry out the linear time history analysis for earthquake loadings. The chosen three ground motions are obtained from the PEER Ground Motion Database using the seismic risk deaggregation results are ChiChi (1999), Kocaeli (1999), and Landers (1992). Furthermore, as required by ASCE 7-16, the ground motions are matched with the site earthquake demand either through uniform or non-uniform scaling. Non-uniform scaling in the form of a spectral matching procedure is used in this research to match the site earthquake demand accurately. In short, the spectral matching procedure is done by modifying the ground motion data such that their acceleration spectrum matches the site earthquake demand from Table A1. The resulting artificial ground motions obtained from the spectral matching procedure may be evaluated in Fig. 6(a). The resulting acceleration response spectrum from each ground motion may then be checked to resemble the site demand spectrum as shown in Fig. 6(b).

The isolation system for the sky bridge connection is modeled using link elements to allow isolated movement for the sky bridges when the two buildings laterally deform due to earthquake excitation (as shown in Fig. 7). As shown, the link elements are modeled by connecting the related nodes in each building with analytical nodes of the sky bridge beams.

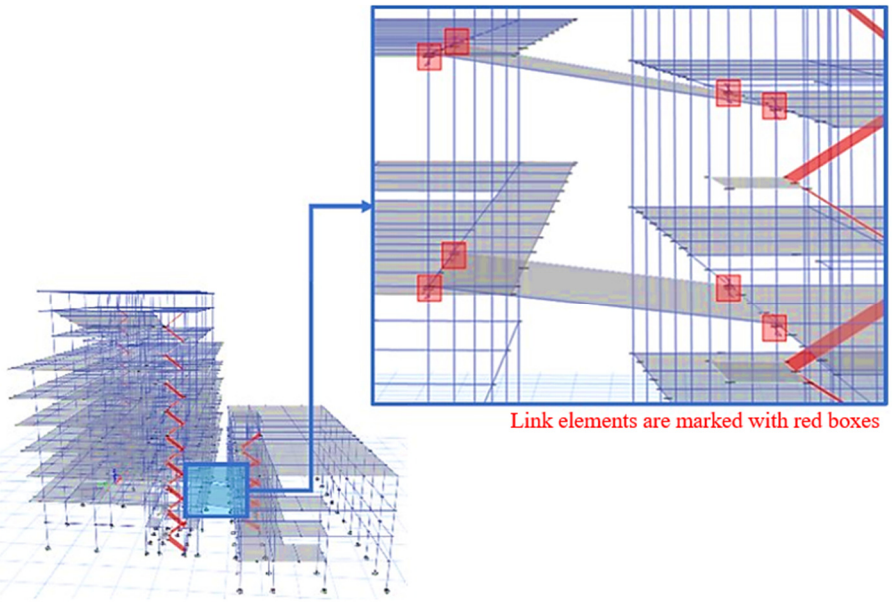

Fig. 7 Position of link elements

The sky bridge modeling is shown in Fig. 8(a), with schematics of the proposed isolation at the ends of the sky bridge shown in Fig. 8(b). Additional degrees of freedom for translation and rotations are introduced at the nodes of the sky bridge connection by its isolated movements. The notation ‘sk’ designates the additional degree of freedom (DOF) of the sky bridge, with the relative vertical deflection constrained to zero. This condition assumes that the isolation is only effective in releasing lateral restraining forces. This choice of constraint is done to resemble bi-directional roller isolation as stated in the introduction. The schematic of the isolation is presented in Fig. 1, inspired by the study of Hosseini and Soroor [12]. Furthermore, the boundary condition is chosen by reflecting on a study by Lee et al. [17].

The research concluded that additional stiffness to a sky bridge isolation system does not drastically affect the dynamic behaviors of two linked structures. It is stated that additional stiffness from the isolation system is trivial when compared to the whole structure stiffness, as the isolation system is used only at the sky bridge connection. Considering this finding, no additional stiffness is put at the isolation system in this research to evaluate the effects of isolation may bring at its extreme. An extended study was conducted to evaluate the local stresses in the sky bridge due to the forces at their ends. The initial

BIM model was transferred to SAP2000 so that the sky bridge could be modeled with solid 3-D elements. This decision was made as the frame element in ETABS could not display a detailed distribution of stresses along the cross-section. The solid 3-D element modeling is limited to the concrete material modeling mainly to evaluate the cracking that may occur.

This study integrated BIM using Autodesk Revit 2023.1 as the BIM software and CSi ETABS v21.0.0.0 for structural analysis and design. CSixRevit 2023.1 served as a plugin for seamless data migration between Autodesk Revit and CSi ETABS. Additionally, Naviate Rebar 2023.1.4 was selected as an additional plugin to enhance reinforcement detailing in the BIM model. The reinforcement volume of structural elements will be obtained from the BIM software of Autodesk Revit.

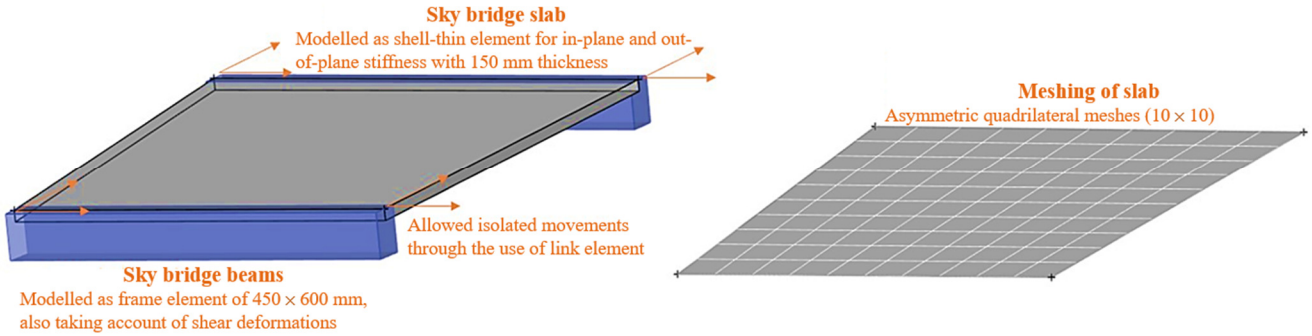

(a) Choices of finite elements

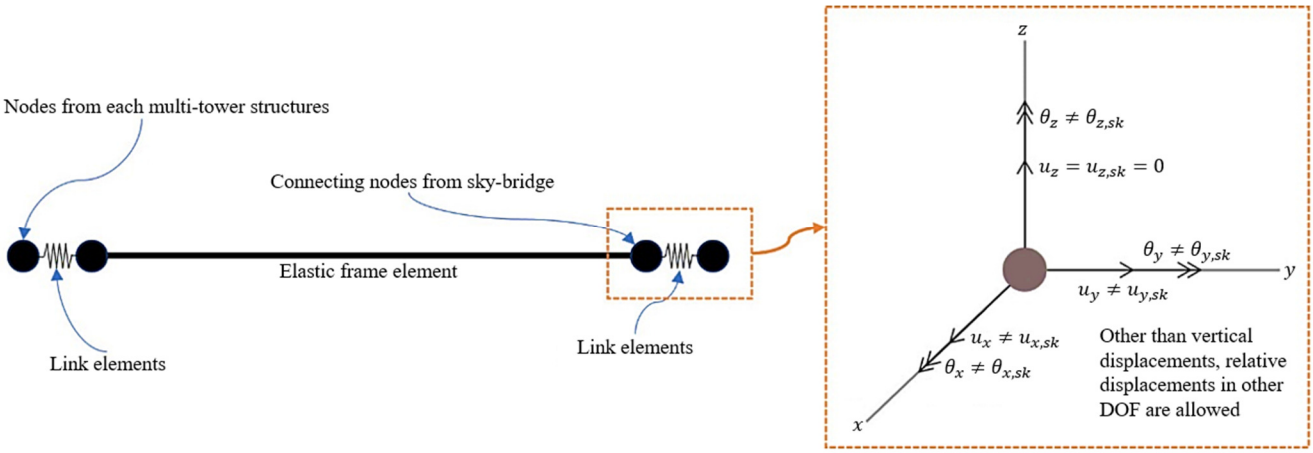

(b) Degree of freedom for the link elements

Fig. 8 Detailed modeling of sky bridge

3. Results and Discussions

An Eigen modal analysis was carried out for both models of the multi-tower building, with and without isolation in the sky bridge connection. From this analysis, a convergence ratio graph depicting the accumulated mass participation in the three main vibration directions of the buildings is presented in Fig. 9. The modal analysis serves as a reference to showcase the dynamic characteristics of a structure under linear conditions. Lower mode numbers signify the fundamental period of the structure and indicate its dominant behaviors during dynamic excitation. Conversely, higher mode numbers reveal the structure's higher vibration properties. The influence of higher mode shapes is known to increase as the complexity of a structure rises.

Fig. 9 illustrates that the rate of mass participation convergence is higher when the isolation system is not employed in the sky bridge connection. However, it should be noted that the convergence rate of the mass participation ratio is not a focal point during modal analysis. This is because the computational efforts required for Eigen modal analysis are insignificant with current hardware capabilities. Evaluating the first few mode shape results presented in Fig. 9, it is evident that mass participation is better defined in lateral directions when the connection isolation is implemented. For clarity, mass participation

is considered better defined as mass participation in a direction that is distinctly defined without interference from other directions. This change in response is considered to benefit the structural design as it simplifies the fundamental dynamic properties of the two buildings. Through simplifying the dynamic properties, predictable behaviors and clear load paths may then be obtained to develop an efficient design.

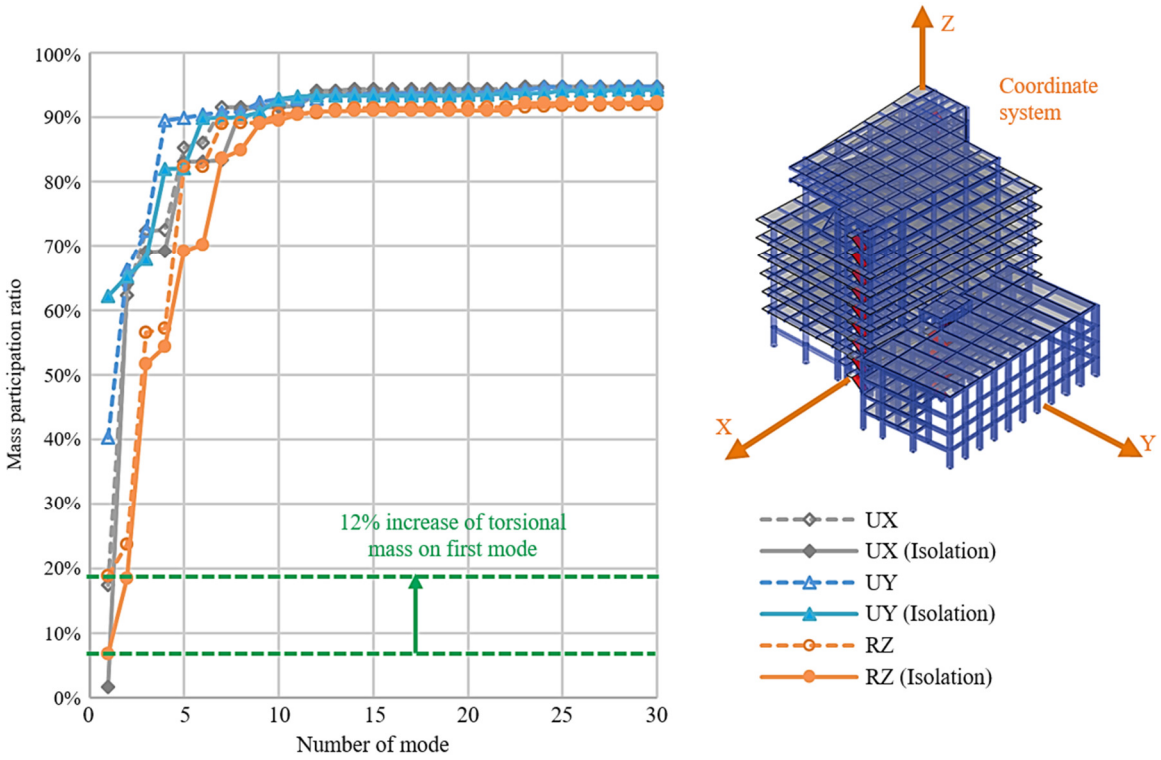

Fig. 9 Convergence plot of cumulative mass participation

Moreover, torsional behavior is significantly more pronounced in the initial mode shapes when no isolation is implemented. As shown in Fig. 9, approximately an increase of 12% in torsional mass participation is seen in the first mode when the isolation is not used. The torsional mass participation is derived from the dynamic equilibrium of a multi-degree-of-freedom system:

$$[M]\{\ddot{u}\}+[C]\{\dot{u}\}+[K]\{u\}=-[M]\{\iota\}\{\ddot{u}_g\} \tag{1}$$

where $[M]$ is the global mass matrix $[C]$ is the global damping matrix, $[K]$ is the global stiffness matrix, $\{u\}$ is the displacement of the structure, and $\{\ddot{u}_g\}$ is the ground acceleration vector. The modal expansion procedure is carried out such that the total dynamic responses of a structure may be uncoupled as combined responses from each modal response. This procedure is known as modal analysis. By doing so, the uncoupled dynamic equilibrium for the response of mode-n is derived:

$$\ddot{q}_n+2\zeta_n\omega_n\dot{q}_n+\omega_n^2 q_n=-\Gamma_n\ddot{u}_g(t) \tag{2}$$

where for each mode n, q_n is the modal coordinate, ζ_n is the modal damping ratio, and ω_n is the radial frequency. During the derivation, some variables are introduced to allow the uncoupling procedure to take place. For instance, a spatial vector $\{s_n\}$ is introduced to express the excitation term contribution previously on each mode:

$$\{s_n\}=\Gamma_n[M]\{\phi_n\} \tag{3}$$

where the factor Γ_n is computed as follows:

$$\Gamma_n=\frac{L_n}{M_n} \tag{4}$$

$$L_n = \sum_{j=1}^{N} m_j \phi_{jn} \tag{5}$$

$$M_n = \{\phi_n\}^T [M] \{\phi_n\} \tag{6}$$

m_j refers to story mass in story j, and $\{\phi_n\}$ is the Eigenvector or mode shape of the building. The full spatial contribution of a structure is simply:

$$\{s\} = [M]\{\iota\} \tag{7}$$

where $\{\iota\}$ is a vector of ones as the entry, symbolizing 100% contribution of mass. Finally, mass participation in each vibrational direction of interest is then calculated as:

$$MPF_n = \frac{\{s_n\}}{\{s\}} \tag{8}$$

which in short translates to the ratio of mass captured in each mode compared to the whole mass of the structure. In conclusion, the torsional mass participation of a mode is the torsional mass captured in a mode, compared to the total mass corresponding to the torsional DOF of the system.

A similar increase in torsional action is also reported by Meng et al. [3]. The research noted that a significant torsional deformation may occur if the height difference between two linked structures is significant, quite resembling the current case study in this paper. The research, however, was done by fully connecting two separate structure floor plans such that all ends of the buildings are linked together. This research further points out that the effect also applies regardless of the area of connection between two multi-tower buildings. Minimizing torsional behavior is advantageous for the dynamic response of a building, given the typically constrained torsional capacity of structural elements.

Conclusively, these phenomena occur due to the significant amplification of the coupling effect between the two buildings when the sky bridge is rigidly connected without an isolation system. A visual representation regarding the coupling effect may be evaluated clearly in Fig. 10. The colors represent magnitudes of unitless displacements (mode shape) obtained through Eigen modal analysis. By comparing Fig. 10(a) to Fig. 10(b), it is evident that coupling effects are reduced through the introduction of isolation.

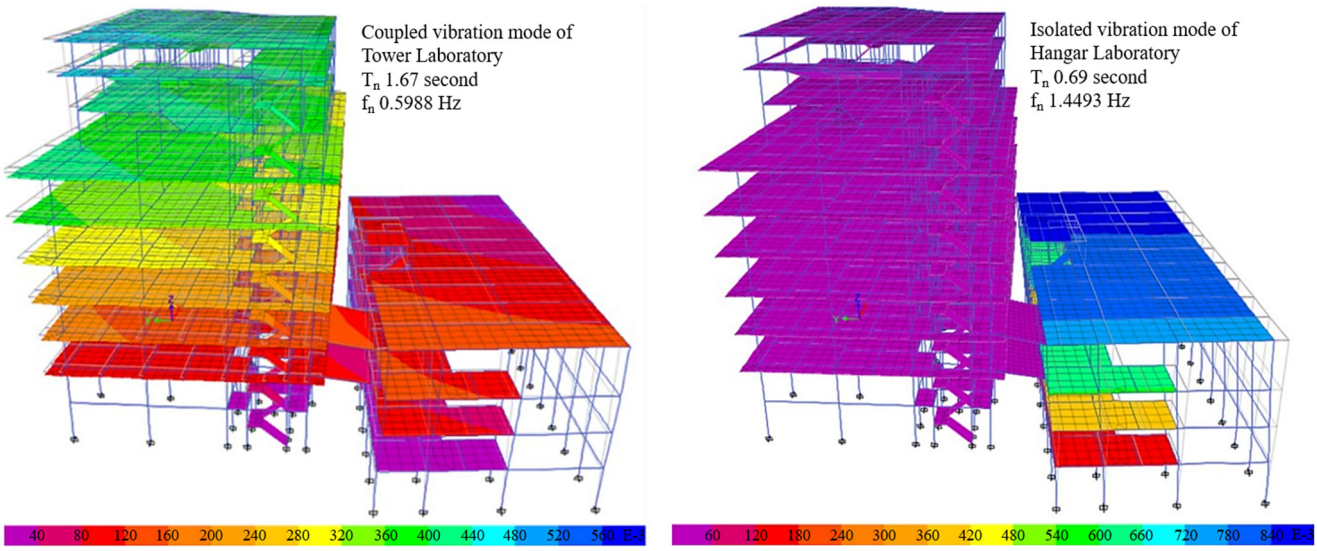

(a) Model without sky bridge connection isolation (b) Model with sky bridge connection isolation

Fig. 10 Mode of vibrations showing mode shapes of the buildings

Fig. 11 shows the total dissipated energy from the two buildings under the three specified ground motions. This total energy encompasses kinetic, potential, and dissipative energy due to damping. Linear analysis is performed in this research, and a constant modal damping ratio of 5% critical is taken for every mode shape response. Taken from the basics of structural dynamics, the balance of energy in a system due to an earthquake ground motion is computed as follows:

$$E_I(t) = E_K(t) + E_D(t) + E_S(t) + E_Y(t) \tag{9}$$

$$E_K(t) = \int_0^u m\ddot{u}(t)du \tag{10}$$

$$E_D(t) = \int_0^t c\left[\dot{u}(t)\right]^2 dt \tag{11}$$

$$E_S(t) = \frac{\left[f_s(t)\right]^2}{2k} \tag{12}$$

$$E_Y(t) = \int_0^u f_s(u)du - E_s(t) \tag{13}$$

where $E_I(t)$, $E_K(t)$, $E_D(t)$, $E_S(t)$, and $E_Y(t)$ in order are the energy input, kinetic energy, damping energy, strain energy, and yield energy at a specific time t. The terms m, c, u, and f_s in order are the system mass, damping, displacements, and resisting force due to the earthquake excitation.

Fig. 11(b) confirms dissipated energy with linear analysis, where most of the energy is dissipated through damping alone. It may be seen from the figure that damping energy contributes about 92.5% of the total dissipated energy at the end of the ChiChi ground motion excitation. The rest of the dissipated energy is then composed of kinetic and strain energy as shown. It is important to note that energy is the product of force and displacement. Therefore, higher dissipated energy is anticipated as shown in Fig. 11(a) in the model incorporating isolation, as the buildings are allowed to move more freely. The reason behind it is due to the higher stiffness in the form of a coupling effect when no isolation is used, leading to fewer displacements in the model without an isolation system. In summary, the energy escalation for the ChiChi, Kocaeli, and Landers ground motions reaches a maximum of 33.3%, 26.9%, and 31.1% respectively at each specific time step.

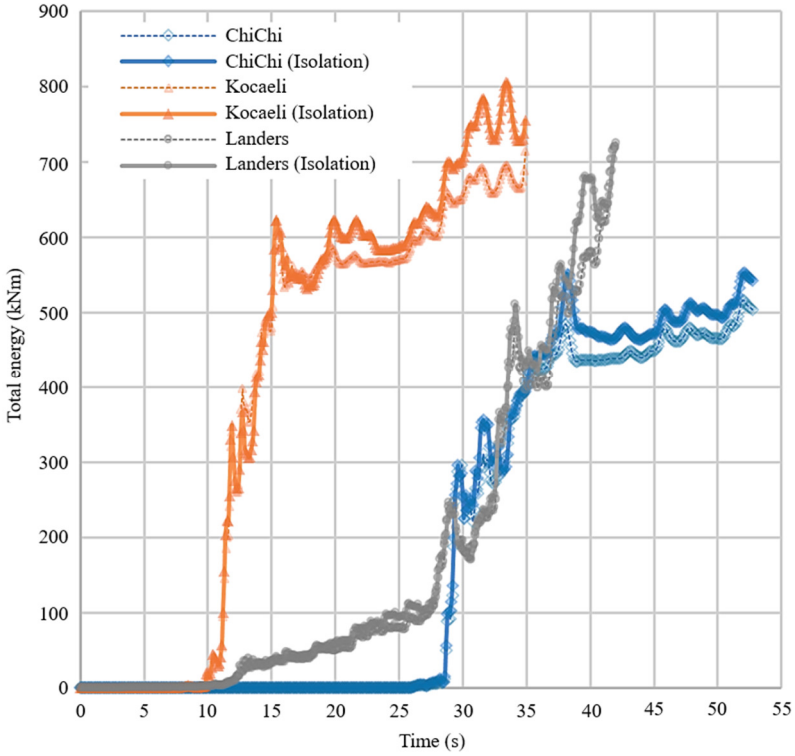

(a) Energy for each ground motion

Fig. 11 Total cumulative energy plot

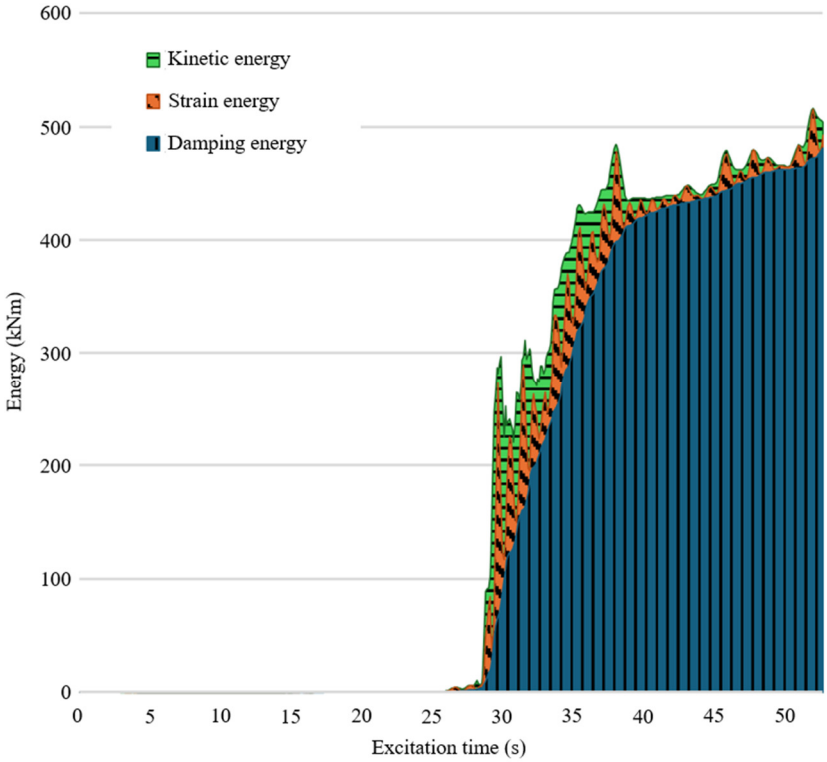

(b) Detailed energy dissipation for ChiChi ground motion under linear analysis

Fig. 11 Total cumulative energy plot (continued)

Fig. 12 presents the spectral displacements of both structures at their respective roof elevations. Spectral displacements serve to depict the dynamic characteristics of a structure when subjected to external dynamic excitation with specific periods. It is crucial to acknowledge that earthquake excitation entails a random occurrence of waves traveling at varying periods. Thus, the actual displacements of a structure are greatly influenced by the characteristics of the ground motion during an earthquake event.

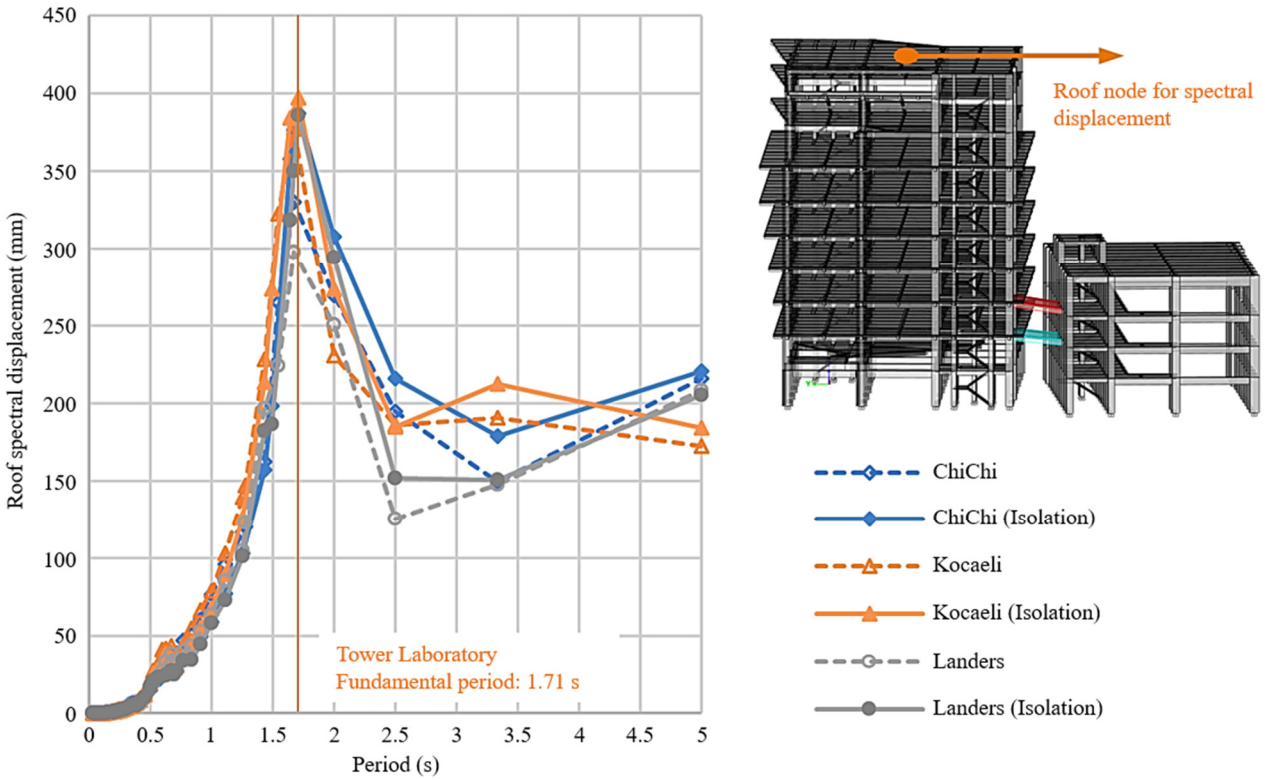

(a) Tower Laboratory building

Fig. 12 Spectral displacements plot

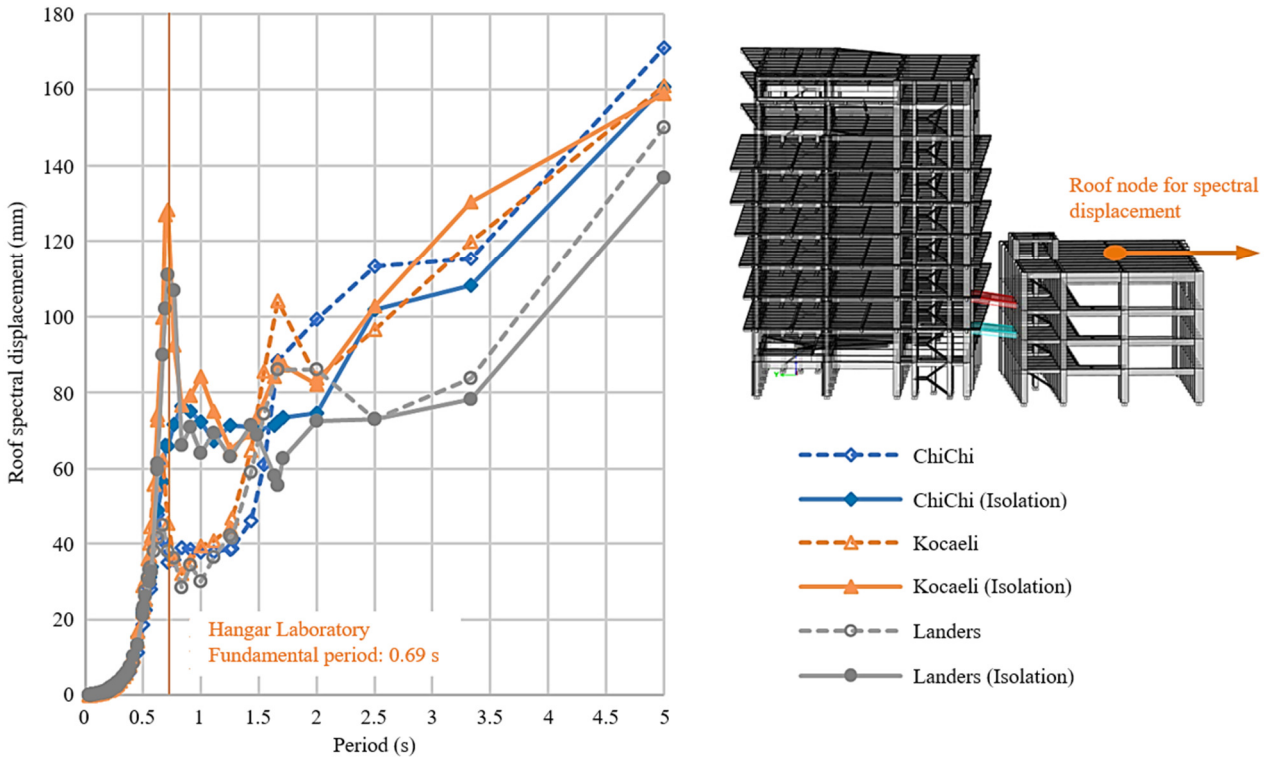

(b) Hangar Laboratory building

Fig. 12 Spectral displacements plot (continued)

Fig. 12(a) presented the roof spectral displacement of the Tower Laboratory building. Under its fundamental period of 1.71 seconds, the utilization of isolation increased the roof spectral displacement by about 14.3% on average. Fig. 12(b) then presented the roof spectral displacement of the Hangar Laboratory building. Under its fundamental period of 0.69 seconds, the roof spectral displacement by about 59.1% on average when the isolation system is employed. It is concluded that the usage of isolation in the sky bridge induces changes in the fundamental dynamic behaviors of two connected buildings. For excitation periods shorter than the building's fundamental period, it is also seen that the sky bridge isolation has a negligible effect on the roof displacements. Such changes in behavior suggest responses from higher vibrational modes of the buildings are practically unchanged regardless of the restraints of the sky bridge connection.

Fig. 13 presents the distribution of maximum story shears on each level of the structures due to ground motions applied in critical directions of the buildings at the maximum time step marked in Fig. 6(a). Unusual lateral force distribution is observed when no isolation system is employed for the sky bridge connection, particularly evident in the Tower Laboratory building, as shown in Fig. 13(a). Unusual lateral force distribution is considered where story shears do not incrementally increase from the roof story to the base level of the building. Diaphragm load transfer is evaluated to be the reason for this phenomenon, as significant load transfer is seen when no isolation is used to the sky bridge connection.

Additionally, it is also apparent that there are reductions in dynamic base shear when the sky bridge connects the two buildings without isolation. A maximum dynamic base shear reduction of 24.3% for the Tower Laboratory building and 2.5% for the Hangar Laboratory building is seen when the isolation is unused. Such behaviors may not be able to be captured when employing static load procedures prescribed by building codes. For instance, the static load procedure outlined in ASCE 7-16 typically results in an incremental increase in story shear until reaching the maximum at the ground level as the static base shear. In essence, these behaviors underscore the necessity for dynamic analyses when encountering such complex structural behavior. Regarding the design procedure, the reduction in dynamic base shear implies a need for higher scale factors to align with the base shear from static load analysis. Consequently, escalation of load demands and reinforcements in structural elements is expected due to the higher scale factor.

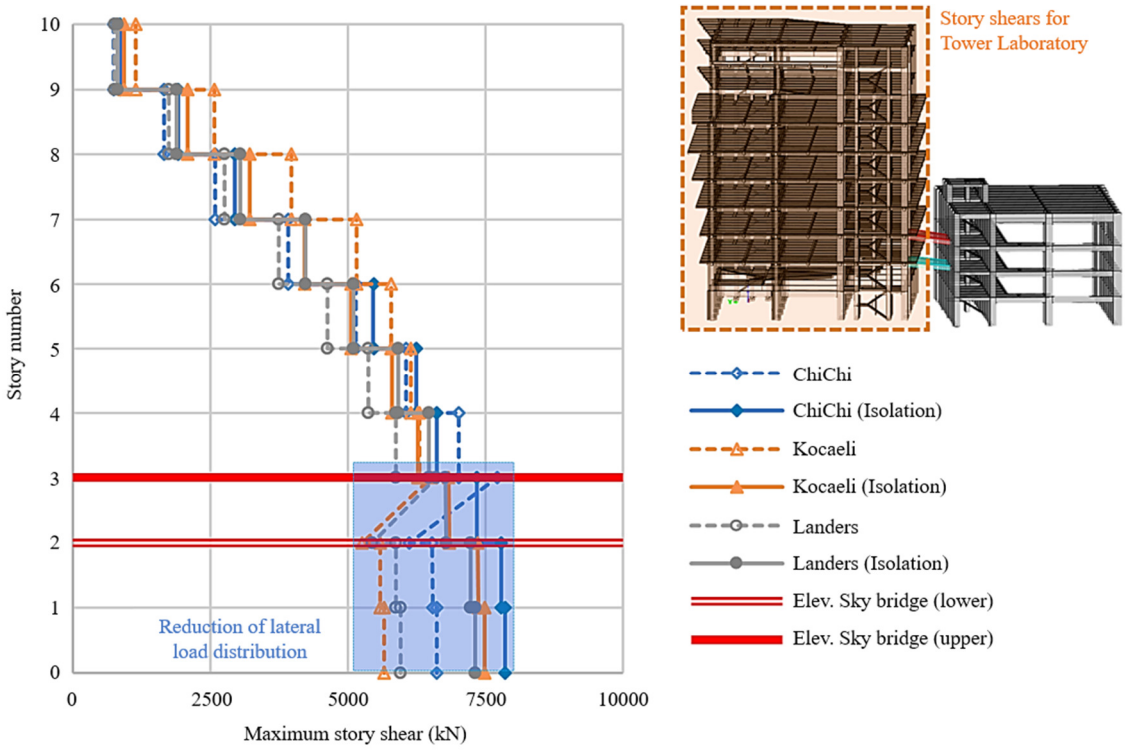

(a) Tower Laboratory building

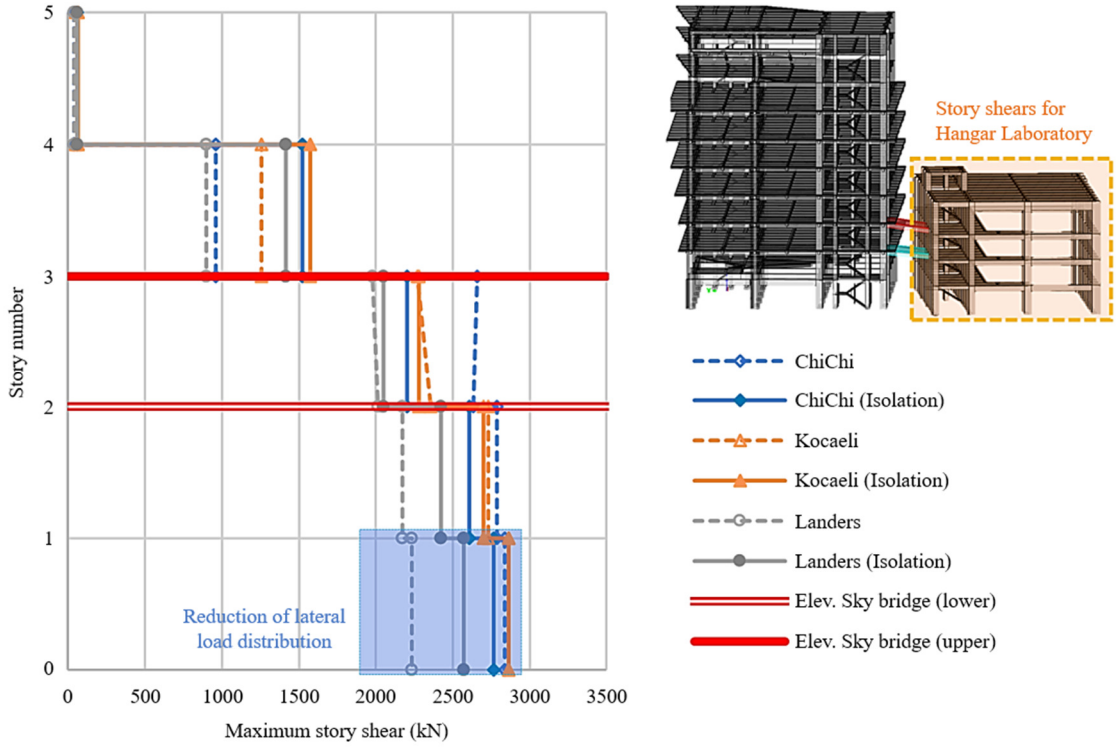

(b) Hangar Laboratory building

Fig. 13 Maximum story shear distribution plot

Fig. 14(a) shows the checking procedure for torsional irregularities complying with ASCE 7-16. According to the code, a building is considered to have torsional irregularity if the maximum drift to the average drift ratio in any level is higher than 1.2. Furthermore, a building is considered to have excessive torsional irregularity if the ratio exceeds 1.4. In the results shown in Fig. 14(b) and Fig. 14(c), a significantly better torsional check result is seen when an isolation system is introduced to the sky bridge connection. Significant reductions of the ratio by a maximum of 12% for the Tower Laboratory building and 15.7% for the Hangar Laboratory building. It shows better torsional behavior from the two buildings when they are allowed to move independently during earthquake excitations.

Such behavior may be explained through observation of the horizontal geometries of the structures as shown in Fig. 4(b). It may be seen that the sky bridge is located at about the outer extreme corner of the two structures. With such positioning, the lateral stiffness of each structure increases at one end only without the isolation (rigidly connected). As a result, more displacements are seen at the other end of the buildings, amplifying the torsional behavior in the process when the sky-bridge is connected without isolation.

For clarity, Fig. 15 highlights the deformed shape of the structure at the maximum time step marked in Fig. 6(a). It may be seen visually that the isolation helps in reducing the torsional effect, specifically during the Kocali and Landers ground motion where significant floor distortion is seen in the Hangar laboratory without the isolation. Regarding design procedures complying with design codes, some benefits of having lower torsional behavior are reduced accidental torsion amplification factors and a smaller redundancy factor of 1.0 which allow for more economical and efficient design.

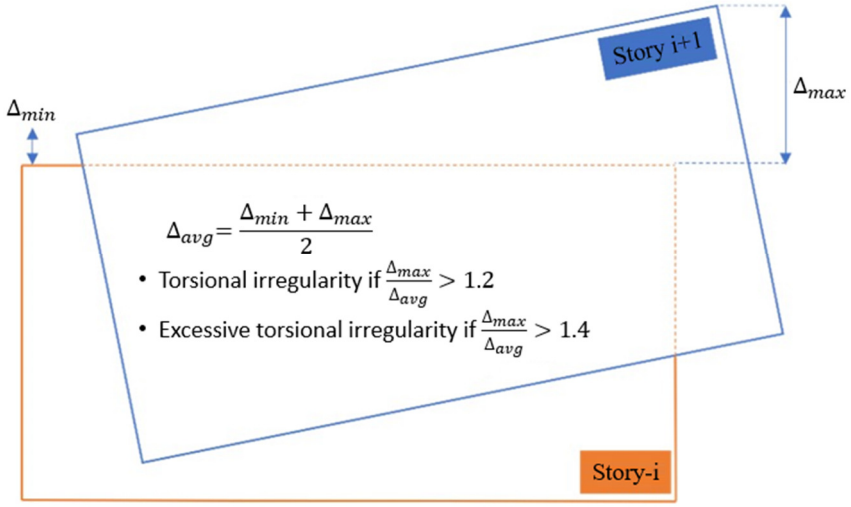

(a) ASCE 7-16's definition of torsional irregularity

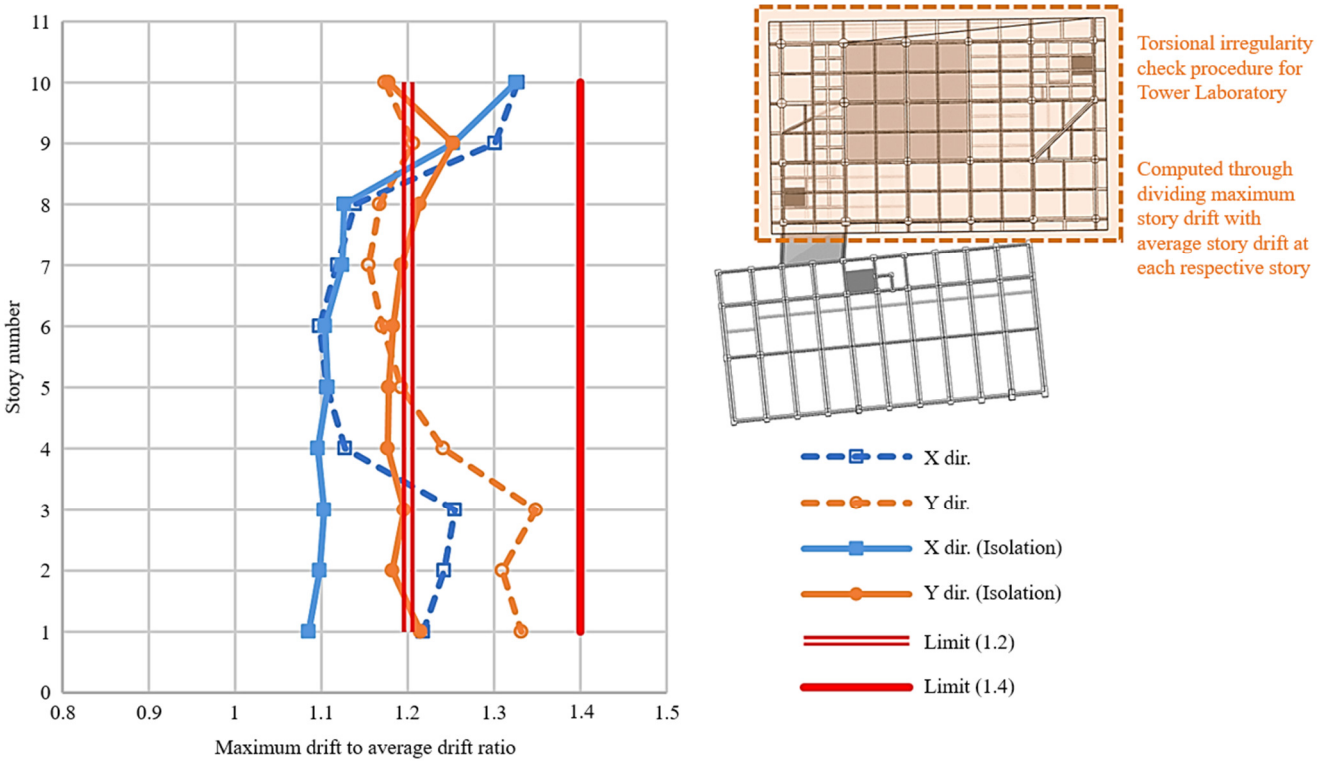

(b) Results for Tower Laboratory building

Fig. 14 Torsional irregularity check

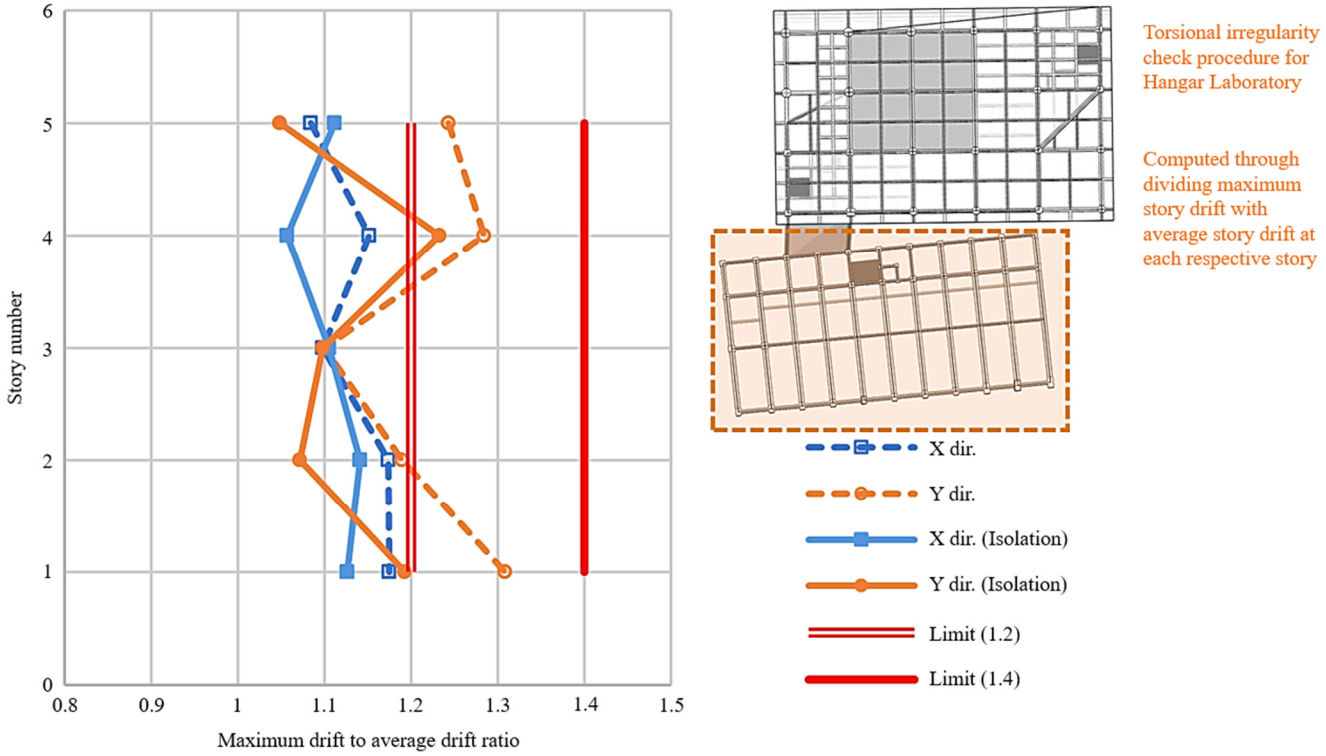

(c) Results for Hangar Laboratory building

Fig. 14 Torsional irregularity check (continued)

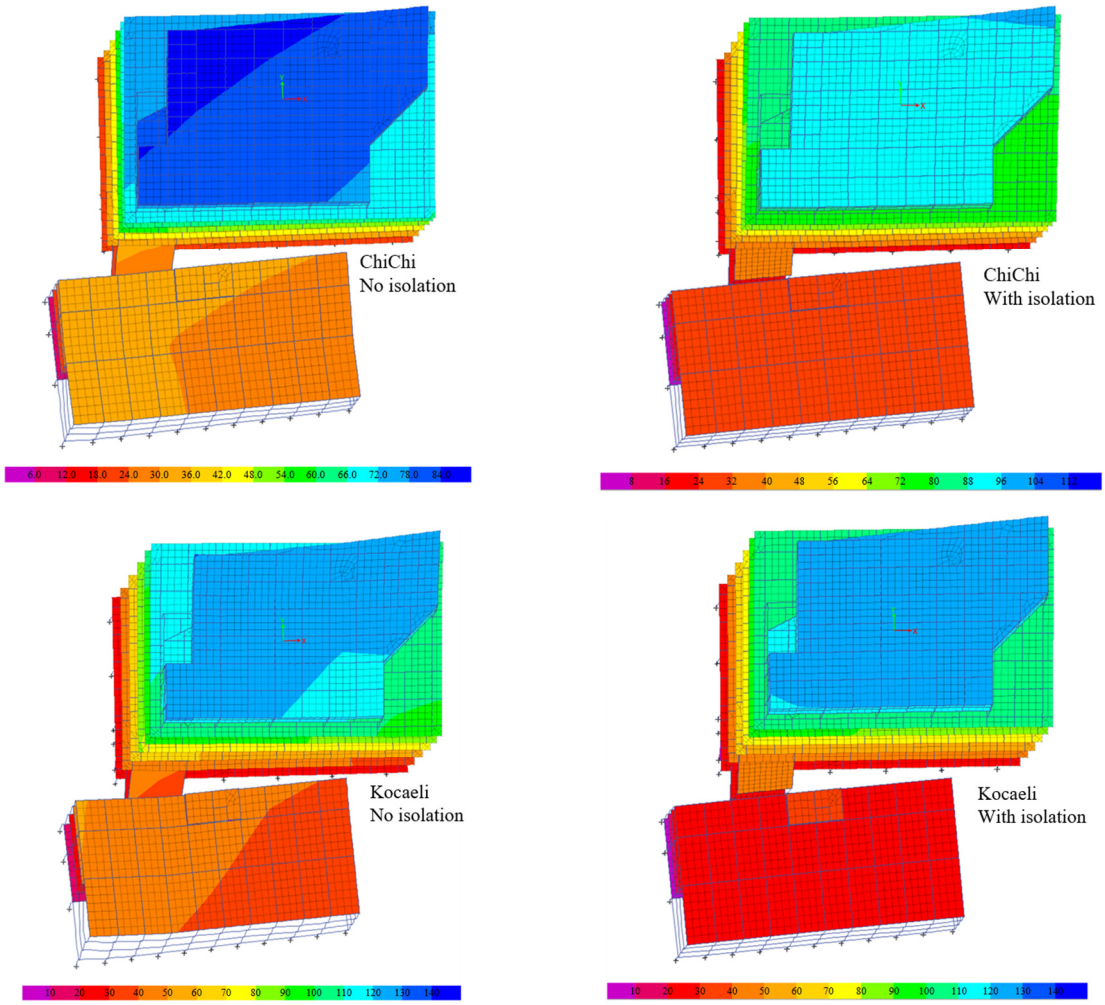

Fig. 15 Maximum deformed shapes due to each ground motion

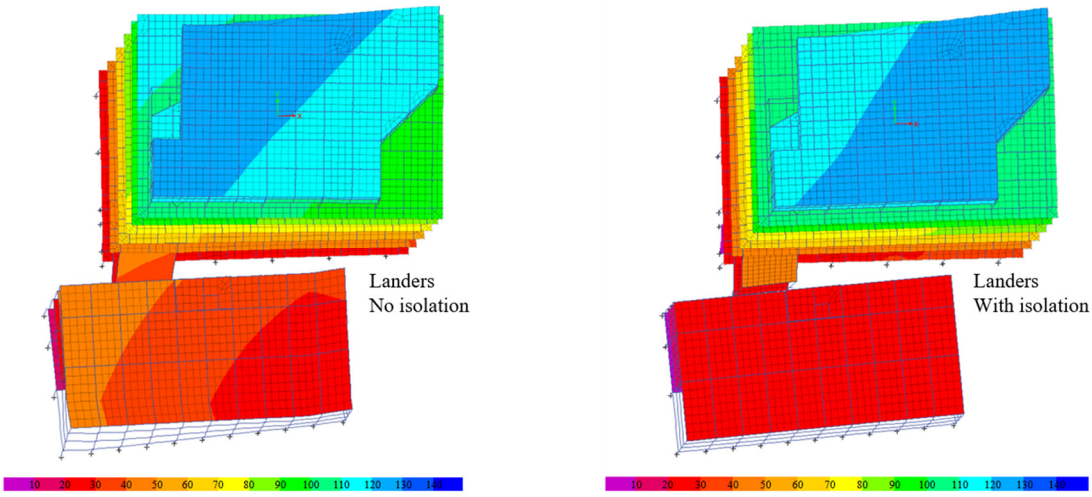

Fig. 15 Maximum deformed shapes due to each ground motion (continued)

Tensile stresses of concrete were an interest to simulate cracking that may occur at the sky bridge system. As mentioned previously, SAP2000 is used for this analysis due to the finite element modeling limitation of ETABS. Fig. 16 displays the stresses that occur at the sky bridge before and after the usage of isolation. A limiting stress of 3.7 MPa is used as the threshold of the stress contour as it relates to the rupture strength of the concrete material. It may be evaluated in Fig. 16(b), that the usage of isolation significantly reduced the stress level at the sky bridge system. The reduced stress is evaluated to be lower than the modulus of rupture of the concrete, implying that cracks at the sky bridge are eliminated through the usage of isolation.

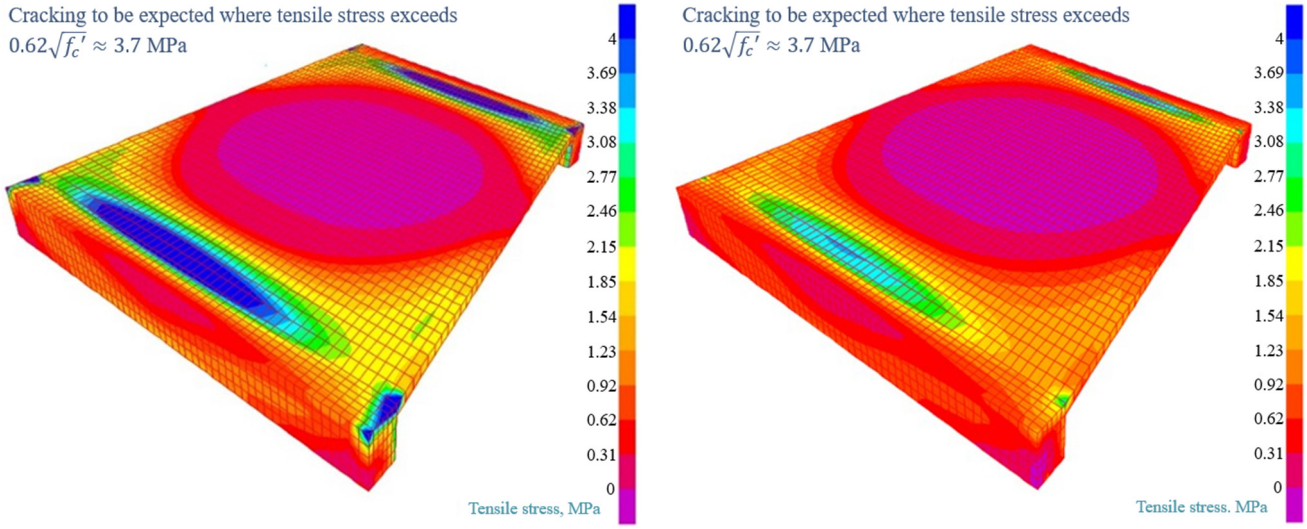

(a) Without isolation (b) With isolation

Fig. 16 State of stresses at the sky bridge element

Design verification and reinforcement design are conducted following the building code, adhering to ACI 318M-14 standards. The reinforcements are designed such that each structural element can resist the required bending, shear, torsional, and axial demands. The detailing for the cross sections of the sky bridge beams based on the required reinforcement areas may be evaluated in Fig. 17. As seen in the figure, a significant reduction of reinforcement is seen upon the usage of movement isolation at the sky bridge connection. The reduction of reinforcement needed is due to reduced load demands and stress transfers when the isolation is introduced, as demonstrated previously. It may be evaluated that the required longitudinal bars decreased significantly, while the required transverse bars did not decrease as significantly. The reason for this is due to the required confinement provisions for axially loaded members as specified in ACI 318M-14 standards governing the design. The reductions of the required reinforcements imply that a more efficient structure both in economical aspects and constructability aspects is obtained by the usage of isolation.

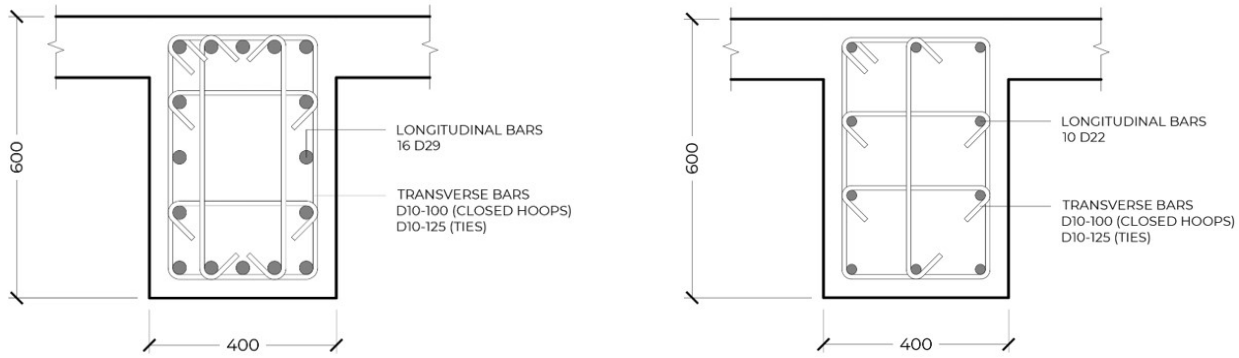

(a) Without isolation (b) With isolation

Fig. 17 Reinforcement details of sky bridge

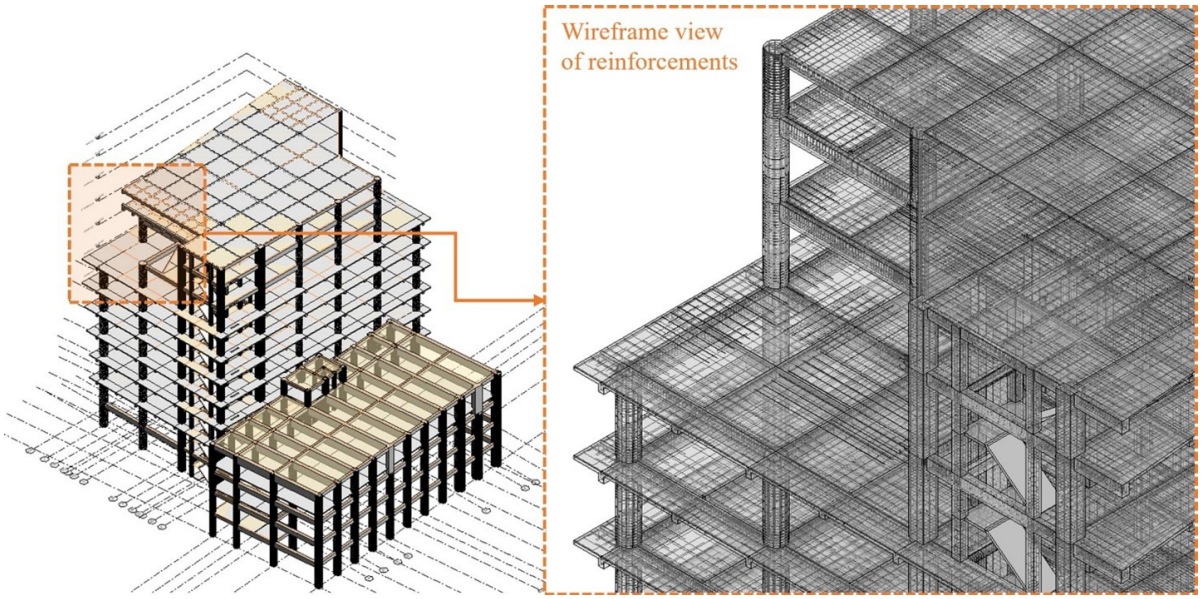

(a) Fully transferred model

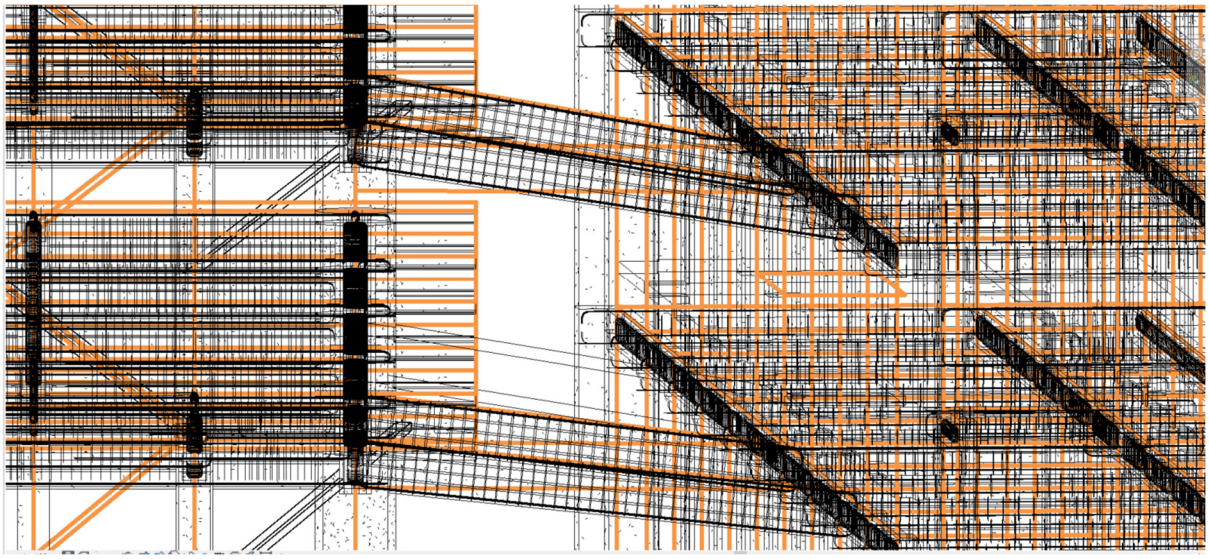

(b) Reinforcement of sky bridge

Fig. 18 Transferred BIM model in Revit

Further reinforcement detailing is performed directly through the ETABS detailing feature to obtain the detailing of each structural element. It is crucial to establish parameters such as development lengths, minimum distances between bars, splicing positions, and other relevant reinforcement detail parameters before the detailing. The parameters must comply with the required detailing provisions of the selected structural system. In this research, the detailing variables were made to comply

with special moment resisting frame provisions as designed. The model with its detailing was then transferred to Autodesk Revit for further output processing. The fully transferred model with the reinforcement detailing may be seen in Fig. 18(a). As shown in the figure, the reinforcement detailing of slabs, columns, and beams is obtained in the wireframe view of the BIM model. For clarity, the reinforcement detailing of the sky bridge element alone is shown in Fig. 18(b). It may be seen visually that the detailing parameters have been correctly imported through the distributions of bars in each element. Conclusively, this procedure demonstrates the BIM capability to optimize the design process through straightforward design presentations.

However, it is noticed that the reinforcement detailing choices that ETABS provided are yet to be considered efficient. ETABS selects reinforcement bar sizes based solely on the limitations of bar distances without considering the potential excess amount of reinforcement required to achieve economic results. The required time for the data migrations is also noted to be substantial. Transferring the model with the reinforcement from ETABS to Autodesk Revit for 3083 frame elements and 932 shell elements takes approximately an hour on average. This reported duration is based on using a computer with an Intel Core i7 processor and 16 GB of memory and may vary depending on hardware specifications and model complexity.

Comparisons of the resulting reinforcement volume calculations through the BIM usage are reported in Table 2 and visualized in Fig. 19. Applying an isolation system to the sky bridge connection reduces total reinforcement volumes by 4.32% for the Tower Laboratory building and 1.98% for the Hangar Laboratory building. This volume calculation results imply that the structure response is marginally better when an isolation system is provided to the sky bridge connection due to the reduction of force demands in the structural elements. More significant changes may be evaluated in the sky bridge element itself. As reported in Table 2, a reduction of the sky bridge's reinforcement volume by 36.91% is seen when the isolation system is used. This volume calculation in the end further demonstrates the advantage of using BIM which allows convenient data processing after the structural design process is finished. Particularly for this research, BIM helps in evaluating the quantities of the required reinforcement volumes using the 3D transferred model.

Table 2 Reinforcement volume calculation

Element	Tower Laboratory building		Hangar Laboratory building		Sky bridge element	
	Without isolation	With isolation	Without isolation	With isolation	Without isolation	With isolation
Beam (kg)	410 200	389 360	73 912	74 170	2613	1249
Column (kg)	129 587	123 510	62 460	60 820	-	-
Slab (kg)	98 215	97 550	18 254	16 570	2363	1890
Total (kg)	638 002	610 420	154 626	151 560	4976	3139
Difference (%)	4.32		1.98		36.91	

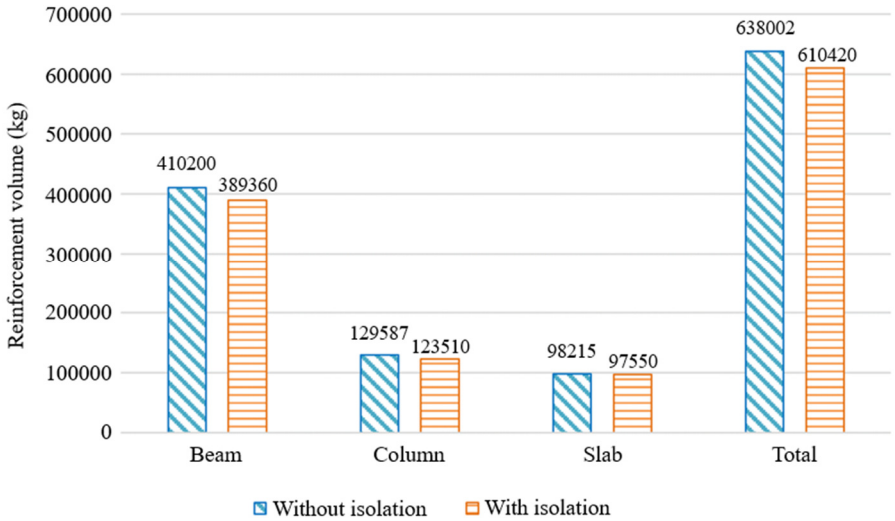

(a) Tower Laboratory building

Fig. 19 Reinforcement volume summary

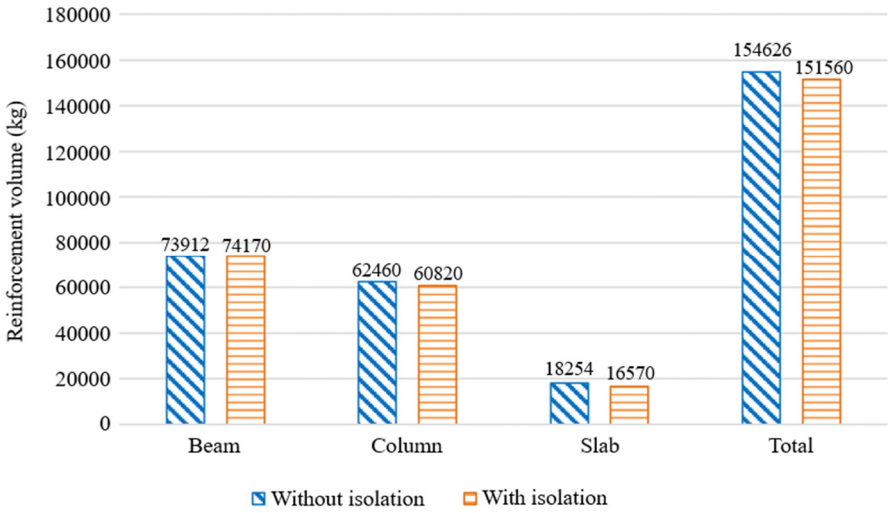

(b) Hangar Laboratory building

Fig. 19 Reinforcement volume summary (continued)

A study from Syukri et al. [28] is used as a benchmark for the reported reinforcement volume. The research is chosen considering the position, size, and function of the building that resembles the Tower Laboratory building from this study. In short, the research presented a BIM-based reinforcement volume calculation of a 5-story laboratory building with an average floor area located in Bengkalis, Indonesia. The research reported on average 34836 kg of beam reinforcement volume per story for the building. Assessing the Tower Laboratory's beam reinforcement volume in Table 2, on average 38936 kg of beam reinforcement volume is obtained per story. Comparing the two results, a marginal difference of 10.53% is seen in the reference results of reinforcement volume. This difference in the reinforcement volume is considered acceptable by taking into account design judgments and the fundamental differences between both buildings. Furthermore, a manual quantity calculation was also done through the structural drawings and the detailing produced previously. A slight error of 5.5% is reported from the manual calculation and is considered to be acceptable due to simplifications that were used during the manual calculation.

4. Conclusions

This paper extends studies in isolation systems for sky bridges by an applied case study of multi-tower building design. Bidirectional isolation systems are applied to the connection of the sky bridge to allow isolated movements during earthquake excitation. Linear time history analysis is used in designing the structures, complying with building codes of ASCE 7-16 and ACI 318M-14. BIM integration is used throughout the study in assisting design visualizations and obtaining accurate volume calculations. Several points that are concluded from this case study are:

(1) Improved torsional behavior is seen when the isolation system is used, such torsional mass participation is reduced by about 12% in the fundamental mode shapes of the buildings.

(2) According to ASCE 7-16, the improvement of torsional behavior is significant enough to reduce the torsional irregularity ratio by up to 15.7%.

(3) More notable benefits that the isolation offers are more predictable dynamic behaviors through independent vibration responses and improved energy dissipation by about 33.3% at maximum.

(4) BIM-based calculation of reinforcement volume reported a substantial reduction of reinforcement volume by 36.91% at maximum when the isolation is used to the sky bridge connection.

Further studies are suggested to fill the limitations that this paper has. A more rigorous analysis, namely non-linear analysis, is recommended to further assess non-linear responses and design optimizations through explicit definitions of material non-linearities. Further studies in assessing other capabilities of BIM are also recommended, as its current state suggests the potential for further research to achieve greater efficiencies in structural designs and broader construction practices.

Acknowledgments

This research is funded by the Directorate of Research and Development, Universitas Indonesia under Hibah PUTI Pascasarjana 2022 (Grant No. NKB-318/UN2.RST/HKP.05.00/2022).

Nomenclature

PEER	Pacific Earthquake Engineering Research Center	DOF	Degree of freedom
ASCE	American Society of Civil Engineers	u_a	Translational DOF at 'a'-axis direction
ACI	American Concrete Institute	θ_a	Rotational DOF at 'a'-axis direction
MCE_R	Maximum considered earthquake risk	UX	Global x-axis translational DOF
F_a	Acceleration-domain site amplification factor	UY	Global y-axis translational DOF
F_v	Velocity-domain site amplification factor	RZ	Global z-axis rotational DOF
S_s	Mapped short-period acceleration parameter	Elev.	Elevation
S_1	Mapped 1-second period acceleration parameter	Dir.	Direction
S_{MS}	MCE_R spectrum response at a short period	I_{gross}	Gross modulus of inertia about a direction
S_{M1}	MCE_R spectrum response at 1-second period	I_{nn}	Modulus of inertia about n-direction
S_{DS}	Design spectrum response in a short period	T_n	Period of mode-n
D_{D1}	Design spectrum response at 1-second period	f_n	Frequency of mode-n
T_0	The initial period for S_{DS}, $0.2S_{D1}/S_{DS}$	T_1	End period for S_{DS}, S_{D1}/S_{DS}

Conflicts of Interest

The authors declare no conflict of interest.

References

[1] S. Y. Jeong, T. H. K. Kang, J. K. Yoon, and R. Klemencic, "Seismic Performance Evaluation of a Tall Building: Practical Modeling of Surrounding Basement Structures," Journal of Building Engineering, vol. 31, article no. 101420, September 2020.

[2] G. Li, H. Zhang, R. Wang, Z. Q. Dong, and D. H. Yu, "Seismic Damage Characteristics and Evaluation of Aboveground-Underground Coupled Structures," Engineering Structures, vol. 283, article no. 115871, May 2023.

[3] F. Meng, X. Ruan, J. Zhao, J. Qiu, L. Meng, and P. Hou, "Analysis of Horizontal Vibration Characteristics of Unequal Height Twin Towers of Rigid Connected Structure," Journal of Building Engineering, vol. 50, article no. 104146, June 2022.

[4] R. Doroudi and S. H. H. Lavassani, "Connection of Coupled Buildings: A State-of-the-Art Review," Structures, vol. 33, pp. 1299-1326, October 2021.

[5] A. Soltanzadeh, H. Mazaherian, and S. Heidari, "The Effects of Cultural Behavior on the Evacuation of the First Residential Towers Built in Iran (Case Study: Saman Twin Towers From the 1970s in Tehran)," Journal of Building Engineering, vol. 76, article no. 107231, October 2023.

[6] S. Mahmoud, "Horizontally Connected High-Rise Buildings Under Earthquake Loadings," Ain Shams Engineering Journal, vol. 10, no. 1, pp. 227-241, March 2019.

[7] X. Chen and J. Xiong, "Seismic Resilient Design With Base Isolation Device Using Friction Pendulum Bearing and Viscous Damper," Soil Dynamics and Earthquake Engineering, vol. 153, article no. 107073, February 2022.

[8] J. M. Jara, E. J. Hernández, and B. A. Olmos, "Effect of Epicentral Distance on the Applicability of Base Isolation and Energy Dissipation Systems to Improve Seismic Behavior of RC Buildings," Engineering Structures, vol. 230, article no. 111727, March 2021.

[9] C. Zhang and A. Ali, "The Advancement of Seismic Isolation and Energy Dissipation Mechanisms Based on Friction," Soil Dynamics and Earthquake Engineering, vol. 146, article no. 106746, July 2021.

[10] M. Teguh, "Structural Behaviour of Precast Reinforced Concrete Frames on a Non-Engineered Building Subjected to Lateral Loads," International Journal of Engineering and Technology Innovation, vol. 6, no. 2, pp. 152-164, April 2016.

[11] K. S. Numayr, R. H. Haddad, Q. D. Ailabouni, and M. A. Haddad, "Passive Base Isolation System for an Asymmetric Building," 7th International Conference on Computational Methods in Structural Dynamics and Earthquake Engineering, COMPDYN, pp. 460-472, June 2019.

[12] M. Hosseini and A. Soroor, "Using Orthogonal Pairs of Rollers on Concave Beds (OPRCB) as a Base Isolation System—Part I: Analytical, Experimental and Numerical Studies of OPRCB Isolators," The Structural Design of Tall and Special Buildings, vol. 20, no. 8, pp. 928-950, December 2011.
[13] S. Jain, S. Pujari, and A. Laskar, "Investigation of One Dimensional Multi-Layer Periodic Unit Cell for Structural Base Isolation," Structures, vol. 34, pp. 2151-2163, December 2021.
[14] K. A. Al-Nahlawi and J. K. Wight, "Beam Analysis Using Concrete Tensile Strength in Truss Models," Structural Journal, vol. 89, no. 3, pp. 284-290, 1992.
[15] Q. M. Shakir and H. K. Hanoon, "Behavior of High-Performance Reinforced Arched-Hybrid Self-Compacting Concrete Deep Beam," Journal of Engineering Science and Technology, vol. 18, no. 1, pp. 792-813, February 2023.
[16] Q. Wu, J. Dai, and H. Zhu, "Optimum Design of Passive Control Devices for Reducing the Seismic Response of Twin-Tower-Connected Structures," Journal of Earthquake Engineering, vol. 22, no. 5, pp. 826-860, 2018.
[17] D. G. Lee, H. S. Kim, and H. Ko, "Evaluation of Coupling–Control Effect of a Sky-Bridge for Adjacent Tall Buildings," The Structural Design of Tall and Special Buildings, vol. 21, no. 5, pp. 311-328, May 2012.
[18] W. Guo, L. Guo, Z. Zhai, and S. Li, "Seismic Performance Assessment of a Super High-Rise Twin-Tower Structure Connected With Rotational Friction Negative Stiffness Damper and Lead Rubber Bearing," Soil Dynamics and Earthquake Engineering, vol. 152, article no. 107039, January 2022.
[19] Z. Zhang, X. Li, B. Chen, and X. Hua, "Closed-Form Optimal Design of the Tuned Inerter Damper (TID) Connecting Adjacent Flexible Buildings," Engineering Structures, vol. 302, article no. 117419, March 2024.
[20] T. Hamidavi, S. Abrishami, and M. R. Hosseini, "Towards Intelligent Structural Design of Buildings: A BIM-Based Solution," Journal of Building Engineering, vol. 32, article no. 101685, November 2020.
[21] K. I. Gartoumi, S. Zaki, and M. Aboussaleh, "Building Information Modelling (BIM) Interoperability for Architecture and Engineering (AE) of the Structural Project: A Case Study," Materials Today: Proceedings, in press. https://doi.org/10.1016/j.matpr.2023.05.408
[22] Z. Ding, S. Liu, L. Liao, and L. Zhang, "A Digital Construction Framework Integrating Building Information Modeling and Reverse Engineering Technologies for Renovation Projects," Automation in Construction, vol. 102, pp. 45-58, June 2019.
[23] A. B. Aragó, J. R. Hernando, F. J. L. Saez, and J. C. Bertran, "Quantity Surveying and BIM 5D. Its Implementation and Analysis Based on a Case Study Approach in Spain," Journal of Building Engineering, vol. 44, article no. 103234, December 2021.
[24] H. Feng, D. R. Liyanage, H. Karunathilake, R. Sadiq, and K. Hewage, "BIM-Based Life Cycle Environmental Performance Assessment of Single-Family Houses: Renovation and Reconstruction Strategies for Aging Building Stock in British Columbia," Journal of Cleaner Production, vol. 250, article no. 119543, March 2020.
[25] S. Kalinichuk and A. Tomek, "Construction Industry Products Diversification by Implementation of BIM," International Journal of Engineering and Technology Innovation, vol. 3, no. 4, pp. 251-258, October 2013.
[26] G. Brooker and H. Lin, "A Twin-Towered High-Tech Headquarters," CTBUH Journal, no. 4, pp. 12-19, 2022.
[27] A. Veall, I. Shleykov, A. Rahimian, and K. Moazami, "Atlantis the Royal the Palm, UAE," International Journal of High-Rise Buildings, vol. 11, no. 1, pp. 51-59, 2022.
[28] A. Syukri, H. Alexander, I. Agus, A. Akbar, R. Bukhari, and D. Hendra, "Quantity Optimization of Structure Works With Building Information Modeling for Politeknik Negeri Padang's Integrated Technology Laboratory Building Design," Proceedings of the 11th International Applied Business and Engineering Conference, pp. 1-10, September 2023.

Appendix

Table A1 Seismic loading parameters
(Mapped parameters adopted from Indonesia's Design Spectrum Response Map)

Parameters	Values
Risk category	IV
Importance factor I_e	1.5

Table A1 Seismic loading parameters (continued)
(Mapped parameters adopted from Indonesia's Design Spectrum Response Map)

Parameters	Values
Site location	Longitude: 106.8274
	Latitude: -6.3605
Mapped acceleration parameters	S_s: 0.891 g
	S_1: 0.419 g
Mapped long period T_L	20 seconds
Site class	Site class E
Site amplification factors	F_a: 1.1871
	F_v: 2.3625
MCE_R spectrum parameters	S_{MS}: 1.0578 g
	S_{M1}: 0.9893 g
Design spectrum parameters	S_{DS}: 0.7052 g
	S_{D1}: 0.6595 g
Design spectrum periods	T_0: 0.187 second
	T_s: 0.935 second
Seismic design category	D
Lateral force resisting system	Special moment resisting frame
Response modification factor R	8
Overstrength factor Ω_0	3
Deflection amplification factor C_d	5.5

Table A2 Seismic risk deaggregation (Adopted from Indonesia's Seismic Hazard Map)

Variables	Values
Return period	2500 years
Earthquake source	All sources
Earthquake magnitude (M)	7-8.5
Earthquake distance (R)	120-200 km
Earthquake mechanisms	Reverse-slip and strike-slip
Shear wave velocity (Vs30)	0-175 m/s
Earthquake duration	Not limited